

Temperature-Dependent Transferred Hyperfine Coupling  
in Ce and Yb Intermetallics

(Ce および Yb 金属間化合物における温度に依存した超微細結合)

Doctor Thesis  
submitted to  
University of Tokyo

by  
Tetsuo Ohama

大濱 哲夫  
Institute for Solid State Physics  
University of Tokyo

1996

①

Temperature-Dependent Transferred Hyperfine Coupling  
in Ce and Yb Intermetallics

(Ce および Yb 金属間化合物における温度に依存した超微細結合)

Doctor Thesis  
submitted to  
University of Tokyo

by  
Tetsuo Ohama  
大濱 哲夫  
Institute for Solid State Physics  
University of Tokyo

1996

### Acknowledgment

I would like to thank Professor Hiroshi Yasuoka for giving opportunity for completing this thesis and his valuable advice. I have learned very much through discussions with him.

I also thank Dr. James L. Smith, Professor Zachary Fisk, Dr. David Mandrus, and Dr. E. V. Sampathkumaran for their carefully prepared samples.

I am especially grateful to Dr. Shigeru Takagi for stimulating discussions on the hyperfine interactions and the magnetism in  $f$  electron systems.

I have greatly benefited from interaction with the members and visitors of Professor Yasuoka's laboratory, Professor Toshinobu Tuda, Professor Masayuki Itoh, Dr. Shinsaku Kambe, Mr. Takato Machi, Professor Takashi Imai, Dr. Yousuke Yoshinari, Dr. Naoki Fujiwara, Dr. Yutaka Itoh, and Dr. Jun Kikuchi. Since I joined the Yasuoka laboratory, I have learned much about magnetism and experimental technique from them.

I have enjoyed interaction with the current students, Atsushi Goto, Kenji Ikushima, Yasuhiro Ueda, and Hideo Iwase.

I would especially like to thank my wife for her patient support.

## Contents

<b>1</b>	<b>Introduction</b>	<b>1</b>
1.1	General Introduction	1
1.2	Ligand Nuclear Resonance in Rare-Earth Intermetallics	2
1.2.1	Transferred Hyperfine Interactions at Ligand Nuclei	2
1.2.2	Nuclear Relaxation at Ligand Nuclei	4
1.3	Magnetic Properties of the $RCu_2Si_2$ compounds	5
1.3.1	$RCu_2Si_2$ Compounds and $ThCr_2Si_2$ Structure	6
1.3.2	$CeCu_2Si_2$	7
1.3.3	$YbCu_2Si_2$	8
1.3.4	$GdCu_2Si_2$	9
1.3.5	$PrCu_2Si_2$	9
1.3.6	$LaCu_2Si_2$ and $YCu_2Si_2$	10
1.4	Scope of This Thesis	10
<b>2</b>	<b>Experimental Procedure</b>	<b>11</b>
2.1	Sample Preparation	11
2.2	NMR Measurements	11
2.3	Magnetic Susceptibility Measurements	13
<b>3</b>	<b>Susceptibility and Knight Shift Measurements</b>	<b>14</b>
3.1	$CeCu_2Si_2$	14
3.2	$YbCu_2Si_2$	18
3.3	$GdCu_2Si_2$	20
3.4	$PrCu_2Si_2$	23
3.5	$YCu_2Si_2$ and $LaCu_2Si_2$	27
<b>4</b>	<b>Discussion on Static Measurements</b>	<b>30</b>
4.1	Transferred Hyperfine Coupling in $GdCu_2Si_2$	30
4.2	Sign of Transferred Hyperfine Coupling	31
4.3	Temperature-Dependent Hyperfine Coupling in $CeCu_2Si_2$ and $YbCu_2Si_2$	31
4.4	<i>f</i> -Ligand Hybridization in $PrCu_2Si_2$	34
<b>5</b>	<b>Nuclear Relaxation Measurements</b>	<b>36</b>
5.1	$CeCu_2Si_2$	36
5.2	$YbCu_2Si_2$	38
5.3	Discussion	40
<b>6</b>	<b>Conclusion</b>	<b>45</b>
	<b>References</b>	<b>48</b>

# 1 Introduction

## 1.1 General Introduction

The problem of localized magnetic moments in a metal has been an attractive subject for a long period. In the investigations of dilute alloys of 3*d* transition metals [1], magnetic resonance of impurity and host nuclei has provided the most reliable technique to study the magnetic response of these systems [2]. The impurity susceptibility was measured by the impurity nuclear hyperfine field, and the dynamic properties of the impurity were studied by its nuclear relaxation measurements. On the other hand, the host nuclear resonance was studied to probe the conduction electron spin polarization around the magnetic impurity; discrete satellites in the NMR spectrum of host nuclei [3] have given a direct evidence of the RKKY spin polarization [4-6]. However, it is essential that several distinct mechanisms contribute to the hyperfine coupling, and that these contributions cannot often be separated. This problem is the major disadvantage of NMR, and more serious for host nuclear resonance. The approach chosen is considering only the Fermi contact interaction between the host nuclei and the conduction electrons, which are spin-polarized by the *s-d* interaction.

It is expected that rare-earth compounds realize the localized moment better, since the 4*f* electron is more localized than the 3*d* electron. While the dilute alloys of rare-earths have been studied from the same point of view as for the transition metal alloys, stoichiometric intermetallic compounds of the rare-earths also have been extensively studied since 1960's. A wide variety of properties which these lattice systems of rare-earth impurities show, such as heavy-fermion behavior and unconventional superconductivity, constitute one of the most attractive issues at present [7, 8].

The NMR measurement is also a powerful technique in investigations of these *f*-electron lattice systems, but the difficulty related with the hyperfine interactions mentioned above also exists. In particular, the much larger atomic hyperfine coupling of 4*f* electrons make it difficult to observe the rare-earth nuclear resonance in the paramagnetic state. Hence nonmagnetic ligand nuclear resonance, instead, has been studied. While the hyperfine interactions in a magnetic ion can be estimated from those in a free atom, the mechanism of the transferred hyperfine coupling at ligand nuclei is complicated and its quantitative analysis is extremely difficult [9]. Consequently the lack of information on the hyperfine coupling is a serious problem for the ligand nuclear resonance.

Despite this disadvantage, the ligand nuclear resonance in the rare-earth intermetallic compounds [10] can be important for the following reasons. First, NMR is a direct probe of the dynamical magnetic properties. Second, in the *f*-electron lattice system, the hybridization of the *f* electrons with the ligand electrons is a key parameter to determine the physical properties of the system. Since this hybridization can be a major mechanism of the transferred hyperfine field, the ligand nuclear resonance is expected to give rich information on the hybridization effect.

The problem discussed in this thesis on the ligand nuclear resonance in the rare-earth intermetallics is temperature-dependent transferred hyperfine coupling, which appears as a deviation from a linear relation of the Knight shift to the magnetic susceptibility. Such temperature dependence in hyperfine coupling was observed at the P and As sites in CeP

and CeAs by Myers and Narath [11]. It was proposed that the crystal-field (CF) splitting is a possible origin. The anisotropy of the hyperfine coupling in YbCu<sub>2</sub>Si<sub>2</sub> was studied by Shimizu *et al.* [12], and the anomaly in the hyperfine coupling was attributed to the cooperation of the CF splitting and an anisotropic spin polarization of the conduction electrons due to the mixing interaction [13]. The temperature-dependent hyperfine coupling was also observed in YbP by Takagi *et al.* [14]. They discussed it quantitatively on the picture of atomic orbitals. In this case, the difference among the hybridization of the CF-split 4*f* orbitals with the ligand 3*p* electrons is essential. On the other hand, the temperature-dependent hyperfine coupling was also reported in the coherent state of the heavy-fermion systems such as CeSn<sub>3</sub>, YbAl<sub>3</sub> and YbCuAl [15]. For these compounds, it has been argued that the CF splitting is not responsible for the temperature dependence, and instead the transferred hyperfine coupling is possibly modified when the system goes to the coherent state. To clarify the mechanism of these temperature-dependent hyperfine coupling is important for understanding of the dynamics as well as the static magnetic properties of the *f*-electron lattice system.

In the present thesis we investigate the transferred hyperfine coupling in the RCu<sub>2</sub>Si<sub>2</sub> (R=La, Ce, Pr, Gd, Yb, and Y) compounds with the common tetragonal structure. The Knight shift and the nuclear relaxation time (*T*<sub>1</sub>) at two distinct sites of Cu and Si are measured in these compounds, and the anisotropy and the site dependence of the hyperfine coupling are studied in detail. The purposes of this study are: 1) to clarify the effects of the CF splitting and the hybridization of the *f*-electrons with the ligand electrons (*f*-ligand hybridization) on the temperature-dependent hyperfine coupling observed in YbCu<sub>2</sub>Si<sub>2</sub> and CeCu<sub>2</sub>Si<sub>2</sub>, and 2) to clarify the effect of the temperature-dependent coupling on the nuclear relaxation at the ligand sites.

## 1.2 Ligand Nuclear Resonance in Rare-Earth Intermetallics

### 1.2.1 Transferred Hyperfine Interactions at Ligand Nuclei

In this subsection we summarize the current understanding of the transferred hyperfine field in rare-earth intermetallics.

The general form of the hyperfine interaction between the nuclear angular momentum *I* and the electronic spin and orbital angular momenta *s* and *l* is

$$\mathcal{H}_{\text{hf}} = 2\mu_{\text{B}}\gamma_{\text{N}}\hbar\frac{\mathbf{l}\cdot\mathbf{I}}{r^3} - \mu_{\text{B}}\gamma_{\text{N}}\hbar\mathbf{s}\cdot\left[\frac{\mathbf{I}}{r^3} - 3\frac{(\mathbf{r}\cdot\mathbf{I})\mathbf{r}}{r^5}\right] + \frac{8\pi}{3}\mu_{\text{B}}\gamma_{\text{N}}\hbar\mathbf{s}\cdot\mathbf{I}\delta(\mathbf{r}), \quad (1.1)$$

where  $\gamma_{\text{N}}$  is the nuclear gyromagnetic ratio. These terms are the orbital, the dipolar, and the contact hyperfine interactions, respectively.

The transferred hyperfine interactions in rare-earth intermetallics can be understood from the point of view of the conduction electron exchange polarization by the *f* electrons. Jaccarino *et al.* measured the Knight shift at the Al sites in the RAl<sub>2</sub> series compounds, and have found that the hyperfine coupling is positive for rare-earth ions with  $J = L - S$  and negative for  $J = L + S$  [16]. They successfully explained this sign inversion using the *s*-*f* exchange interaction

$$\mathcal{H}_{sf} = -(g_J - 1)J_{sf}\mathbf{J}\cdot\mathbf{s}, \quad (1.2)$$

assuming a negative *s*-*f* exchange parameter  $J_{sf}$ . In the lattice system of the *f* electrons, the interaction between the *f* moment  $\mathbf{J}_j$  and the conduction electron spin  $\mathbf{s}_i$  has the form

$$\mathcal{H}_{sf} = -(g_J - 1)J_{sf}\sum_j\mathbf{J}_j\cdot\mathbf{s}_i\delta(\mathbf{r}_i - \mathbf{R}_j), \quad (1.3)$$

and the Fourier transform of the effective field that each conduction electron experiences is given by

$$\begin{aligned} \mathbf{H}_{\text{eff}}(\mathbf{q}) &= -\frac{(g_J - 1)J_{sf}}{g\mu_{\text{B}}V}\sum_j\mathbf{J}_je^{i\mathbf{q}\cdot\mathbf{R}_j} \\ &= -\frac{(g_J - 1)J_{sf}}{g\mu_{\text{B}}}\langle\mathbf{J}\rangle\sum_{\mathbf{G}}\delta(\mathbf{q} - \mathbf{G}), \end{aligned} \quad (1.4)$$

where  $\mathbf{G}$  is a reciprocal lattice vector. The  $\mathbf{q}=0$  term is a spatially uniform field, and its contribution to the Knight shift via the hyperfine coupling  $A_c$ , between the conduction electrons and the ligand nuclei, is

$$\begin{aligned} K_f &= A_c\chi_c J_{sf}\frac{g_J - 1}{gg_J\mu_{\text{B}}^2}n_f \\ &= K_c J_{sf}\frac{g_J - 1}{gg_J\mu_{\text{B}}^2}n_f, \end{aligned} \quad (1.5)$$

where  $\chi_f/n_f$  is the *f*-electron susceptibility for the rare-earth ion,  $\chi_c$  is the conduction electron susceptibility, and  $K_c$  is the Knight shift due to the conduction electrons without the polarization due to the *f* electrons. Eq. (1.5) may be written as

$$K_f = A_f\frac{\chi_f}{\mu_{\text{B}}n_f}, \quad (1.6)$$

$$A_f = A_c\chi_c J_{sf}\frac{g_J - 1}{gg_J\mu_{\text{B}}}, \quad (1.7)$$

where  $A_f$  is the transferred hyperfine coupling, which is experimentally measured. This formula shows that the factor  $(g_J - 1)$  will cause the sign inversion of the transferred hyperfine coupling. The hyperfine coupling  $A_c$  can be anisotropic due to the dipolar hyperfine coupling between the conduction electrons and the ligand nuclei. Further, when there are some inequivalent ligand sites,  $A_c$  will be different at the individual sites. Thus the anisotropy and the site dependence of the transferred hyperfine coupling  $A_f$  can arise from those of  $A_c$ .

The  $\mathbf{G}\neq 0$  terms in eq. (1.4) can be comparable to the uniform term, and then can make an oscillatory polarization. Further, the hyperfine coupling between the conduction electrons and the ligand nuclei may be modified because the  $\mathbf{q}\neq 0$  components of  $A_c(\mathbf{q})$  must be taken into account. These effects will also appear as the site dependence of the transferred hyperfine coupling. The site dependence was actually observed for two inequivalent Pt sites in the RPt<sub>5</sub> series [17].

The negative exchange parameter deduced experimentally is incompatible with real exchange integrals, which contribution should be positive. Effective exchange interaction

has been theoretically investigated for real rare-earth metals [18]. Watson *et al.* showed that the negative contribution of the mixing interaction [19] between the  $f$  and the conduction electrons can overcome the positive exchange contribution [20]. It was also shown that the effective  $s$ - $f$  exchange parameter can be anisotropic. This anisotropy leads to an anisotropic hyperfine coupling via the conduction electron polarization.

While Watson *et al.* estimated the effective exchange parameter in eq. (1.2), Coqblin and Schrieffer derived a different form of the interaction Hamiltonian for the mixing interaction for the  $f^1$  configuration [13],

$$\mathcal{H}_{CS} = - \sum_{kk'mm'} J_{kk'} c_{k'm'}^\dagger f_m^\dagger f_{m'} c_{km}, \quad (1.8)$$

where  $f_m^\dagger$  is the creation operator for a localized  $f$  electron of  $j = \frac{5}{2}$  and the  $z$  component  $m$ , and  $c_m^\dagger$  is the creation operator for a conduction electron of a partial wave function of wave number  $k$ ,  $j = \frac{5}{2}$  and the  $z$  component  $m$ . This interaction also leads to the anisotropic spin polarization of the conduction electrons. Shimizu *et al.* attributed the anomalous behavior of the transferred hyperfine coupling in  $\text{YbCu}_2\text{Si}_2$  to this anisotropic polarization [12].

It was shown that the anisotropic RKKY-type interaction between two Ce moments arises from this mixing interaction eq. (1.8). An extension for the  $f^n$  case was made [21], and the anisotropic magnetic response in Ce and actinide compounds has been studied.

The transferred hyperfine interaction has been also investigated from the point of view of atomic orbitals [9]. This approach has an advantage in consideration of the hyperfine coupling at ligand nuclear sites. Watson and Freeman calculated the ligand spin polarization in insulating  $\text{GdF}_3$  with the unrestricted Hartree-Fock theory [22]. They revealed that the covalency and overlap between the  $F 2s$  orbital and the  $Gd 5s$  and  $5p$  closed shells give the dominant contribution, and further that the  $4f$  direct overlap contribution is very small. Kasuya argued that these closed shells give an important contribution to the exchange interaction between the  $4f$  and the conduction electrons in the  $Gd$  metal [18]. Since the  $4f$  orbital lies inside the  $5s$  and  $5p$  orbitals, it is plausible to suspect that the above mechanisms, the spin polarization of these closed shells give the important contribution to the transferred hyperfine coupling generally in the rare-earth compounds.

Takagi *et al.* discussed the temperature-dependent hyperfine coupling in  $\text{YbP}$  with the anisotropic mixing [23] of the  $4f$  orbitals with  $3p$  orbitals at the P sites [14]. The  $J = \frac{7}{2}$  multiplet is split into two doublets  $\Gamma_6$ ,  $\Gamma_8$  and a quartet  $\Gamma_7$  in  $\text{YbP}$ . It was shown that the mixing matrix elements for these CF states and the  $p$  orbitals at P sites are different, and that that for the ground  $\Gamma_6$  state is the largest. When the occupation of the CF states varies with temperature, the transferred hyperfine coupling will vary accordingly. This mechanism contradicts the above argument on the outer shell contributions. It seems that this suggests the hyperfine coupling in  $\text{YbP}$  is anomalous in this sense.

### 1.2.2 Nuclear Relaxation at Ligand Nuclei

In general, the nuclear relaxation rate  $1/T_1$  is related to the fluctuating hyperfine field

$\mathbf{H}_{\text{hf}}(t)$  by [24]

$$\frac{1}{T_1} = \frac{\gamma_N^2}{2} \int_{-\infty}^{\infty} dt e^{i\omega_N t} \langle \{ H_{\text{hf}}^+(t) H_{\text{hf}}^-(t) \} \rangle, \quad (1.9)$$

where  $H_{\text{hf}}^\pm = H_{\text{hf}}^x \pm iH_{\text{hf}}^y$ ,  $\{AB\} = (AB + BA)/2$ ,  $\gamma_N$  is the nuclear gyromagnetic ratio, and  $\omega_N$  is the NMR frequency. When the hyperfine field is written with the hyperfine coupling tensor  $\mathbf{A}_i$  and the  $f$  electron angular momentum  $\mathbf{J}_i$  as

$$\begin{aligned} \mathbf{H}_{\text{hf}} &= g \sum_i \mathbf{A}_i \mathbf{J}_i \\ &= g \sum_q \mathbf{A}_q \mathbf{J}_q, \end{aligned} \quad (1.10)$$

where  $\mathbf{A}_q$  and  $\mathbf{J}_q$  are the Fourier transforms of  $\mathbf{A}_i$  and  $\mathbf{J}_i$ , respectively, we obtain

$$\frac{1}{T_1} = \frac{\gamma_N^2 k_B T}{2\mu_B^2} \sum_q |A_{\perp}^q|^2 \frac{\chi_{\perp}''(q, \omega_N)}{\omega_N}. \quad (1.11)$$

When  $\chi(q, \omega)$  is described with a Lorentzian form

$$\chi(q, \omega) = \frac{\chi(q)}{1 - i\omega/\Gamma(q)}, \quad (1.12)$$

the nuclear relaxation rate becomes

$$\frac{1}{T_1} = \frac{\gamma_N^2 k_B T}{2\mu_B^2} \sum_q |A_{\perp}^q|^2 \frac{\chi_{\perp}(q)}{\Gamma(q)}. \quad (1.13)$$

If the spatial correlation of the magnetic moments is weak, we obtain a conventional form

$$\frac{1}{T_1} = \frac{N\gamma_N^2 k_B T}{2\mu_B^2} A_{\perp}^2 \chi_{\perp} \tau, \quad (1.14)$$

where  $\tau = 1/\Gamma$  is the effective fluctuation rate of the magnetic moment. This form is often used for the analysis of experimental data, but it is inadequate for real systems where the CF splitting exists for the following reasons: 1) The dynamical susceptibility cannot be written as eq. (1.12) with the static susceptibility, even when the low-energy part can be described by a Lorentzian form. 2) The anisotropies of the dynamical susceptibility and the hyperfine coupling, must be considered; this has been often neglected. 3) The hyperfine coupling is temperature-dependent in a case, as discussed so far. These problems will be discussed in Sect. 5.

### 1.3 Magnetic Properties of the $\text{RCu}_2\text{Si}_2$ compounds

For long decades, a lot of experiments have been performed on the rare earth intermetallics with the  $\text{ThCr}_2\text{Si}_2$  tetragonal structure [25] to investigate the valence instability of the rare earth ion [26]. In the  $\text{RCu}_2\text{Si}_2$  series, anomalous properties were reported for  $\text{CeCu}_2\text{Si}_2$ ,  $\text{SmCu}_2\text{Si}_2$ ,  $\text{EuCu}_2\text{Si}_2$ , and  $\text{YbCu}_2\text{Si}_2$ . In particular,  $\text{CeCu}_2\text{Si}_2$ , the only cerium heavy-fermion superconductor, has been extensively studied.

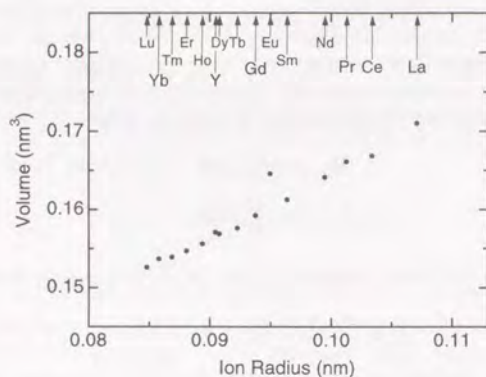


Figure 1.1. Unit cell volume of  $RCu_2Si_2$  compounds vs ionic radius at room temperature [27], Y [28]).

In this study, we have investigated the temperature-dependent hyperfine coupling in  $CeCu_2Si_2$  and  $YbCu_2Si_2$ .  $CeCu_2Si_2$  is characterized by a large CF splitting of a few hundreds K and low Kondo temperature  $T_K \sim 10K$ , while  $YbCu_2Si_2$  is by a CF splitting of the same order and higher  $T_K$ . We chose  $PrCu_2Si_2$  and  $GdCu_2Si_2$  as reference compounds; in  $PrCu_2Si_2$  the CF splitting is small, and in  $GdCu_2Si_2$  one-ion anisotropy is negligible.

To investigate the character of the conduction electrons without  $4f$  electrons, we also studied the Y and La compounds. Since the unit cell volumes of the compounds studied here vary with the rare-earth ionic radii as shown in Fig. 1.1, the character of the conduction electrons may change significantly. Thus these two compounds with different volumes were studied.

Brief reviews on the magnetic properties of these compounds will be given in the following subsections.

### 1.3.1 $RCu_2Si_2$ Compounds and $ThCr_2Si_2$ Structure

The  $ThCr_2Si_2$  tetragonal structure is shown in Fig. 1.2. The separation between the rare-earth ions is relatively large, and it is expected that the direct  $f-f$  coupling is weak. This structure has some advantages for investigation of the transferred hyperfine coupling. First, because rare-earth ions occupy a set of crystallographically equivalent sites, all the rare-earth ions have the identical size of magnetic moments, and it can be estimated from the magnetic susceptibility. Second, because of relatively high local symmetry of the rare-earth, Cu, and Si sites, the bulk susceptibility, the one-ion susceptibility and the Knight shifts at the Cu and Si sites have the identical principal axes. Furthermore, these

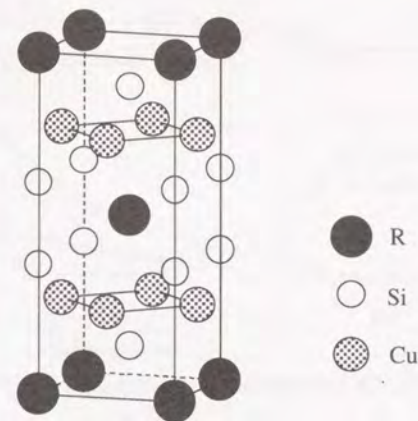


Figure 1.2.  $ThCr_2Si_2$  type structure.

are uniaxially anisotropic, thus the precise measurements are possible with magnetically aligned powder samples. For these reasons, the  $ThCr_2Si_2$  structure is ideal for our purpose.

### 1.3.2 $CeCu_2Si_2$

$CeCu_2Si_2$  is a heavy-electron system which has been intensively investigated because of its unusual superconducting properties [7, 8]. Its complicated  $H-T$  diagram has not been clarified yet [29].

The magnetic susceptibility measured with single crystals shows a Curie-Weiss behavior with anisotropy [30, 31]. From inelastic neutron-scattering measurements, a large CF splitting was suggested; the energy splitting between the first excited and the ground levels is a few hundreds K [32, 33]. Two different CF level schemes for the  $J = 5/2$  multiplet of  $Ce^{3+}$  were proposed by Horn *et al.* (HH) [32] and by Goremychkin and Osborn (GO) [33] as shown in Fig. 1.3. Mean-field calculation with the resulting CF parameters roughly reproduced the anisotropic susceptibility.

In  $CeCu_2Si_2$ ,  $T_K$  has been estimated to be of the order of 10K from several experimental data; for example, a specific-heat measurement [34] and a neutron scattering measurement [32].

The  $^{29}Si$  [35, 36] and  $^{63}Cu$  [37] Knight shifts have already been reported, but these measurements were limited to low temperatures, or the anisotropy was not measured. Aarts *et al.* argued that the "isotropic" part of the hyperfine coupling at the Si sites changes as temperature below 7K, and that this anomaly may be attributed to the formation of the heavy Fermi liquid state [35]. Far above  $T_K$ , the temperature-dependent hyperfine

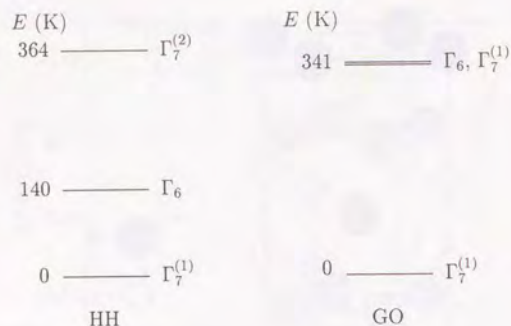


Figure 1.3. CF level schemes for  $\text{CeCu}_2\text{Si}_2$ , see Sect. 3.1.

coupling has been observed at both the sites [38]. The results will be presented in Sect. 3.

The nuclear relaxation measurements have also been reported. From the  $^{29}\text{Si}$   $T_1$  measurement above  $T_K$  [35], it was estimated that the effective relaxation rate of the Ce magnetic moments increases linearly with temperature. On the other hand, the neutron scattering measurement indicated that the quasi-elastic line width changes roughly as  $\sqrt{T}$  [32]. This disagreement is an important problem for understanding of the dynamics.

### 1.3.3 $\text{YbCu}_2\text{Si}_2$

$\text{YbCu}_2\text{Si}_2$  has long been known to be a valence fluctuation system with the Yb valence of 2.9 [39]. Photoemission measurements were made on this compound to examine the Kondo resonance in the single-impurity Anderson model [40, 41], and it was that the Yb valence was 2.9 [40] or 2.55 [42]. A quite large  $\gamma \sim 210\text{mJ/molK}^2$  was reported [43], but no detailed data has been previously published.

The CF splitting of the  $J = \frac{7}{2}$  multiplet of  $\text{Yb}^{3+}$  into four doublets is expected for the  $D_{4h}$  symmetry at the Yb sites. An inelastic neutron-scattering measurement with a powder sample [44, 45] proposed that the excited doublets lie at 18, 23, and 31 meV (Fig. 1.4). The quasi-elastic line width of 4-5meV suggested  $T_K$  of the order of 50K [44]. They reported that the line width seems temperature-independent in  $\text{YbCu}_2\text{Si}_2$ .

Shimizu *et al.* have measured the  $^{63}\text{Cu}$  Knight shift and the magnetic susceptibility with a single crystal [12]. The anisotropic susceptibility is shown in Fig. 1.4. They observed that the hyperfine coupling at the Cu sites significantly changes around 100K. They attributed the temperature-dependent coupling to the mixing between the 4f moments and the conduction electrons.

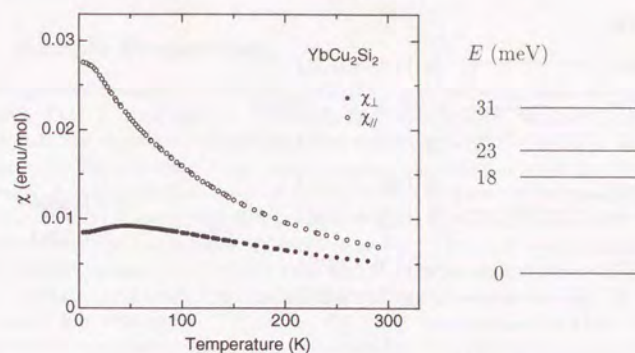


Figure 1.4. Magnetic susceptibility of  $\text{YbCu}_2\text{Si}_2$  single crystal [12], in the basal plane ( $\chi_{\perp}$ ) and along the  $c$ -axis ( $\chi_{\parallel}$ ). CF level scheme [44, 45] is also shown.

### 1.3.4 $\text{GdCu}_2\text{Si}_2$

$\text{GdCu}_2\text{Si}_2$  is an antiferromagnetic metal with the Néel temperature ( $T_N$ ) of 12K [46]. The magnetic susceptibility measured with a powder sample follows a Curie-Weiss law with the effective moment of  $7.75\mu_B$ , close to the free  $\text{Gd}^{3+}$  value of  $7.94\mu_B$ .

### 1.3.5 $\text{PrCu}_2\text{Si}_2$

$\text{PrCu}_2\text{Si}_2$  is an antiferromagnetic metal with  $T_N \sim 21\text{K}$  [47]. The magnetic susceptibility measured with a powder sample follows a Curie-Weiss law with the effective moment of  $3.6\mu_B$  [48], close to the free  $\text{Pr}^{3+}$  value of  $3.58\mu_B$ . It has been known that the valence of Pr occasionally deviates from three. However, the unit cell volume of  $\text{PrCu}_2\text{Si}_2$  lies on the smooth curve of other trivalent compounds in Fig. 1.1, we thus expect that the Pr ions are trivalent in  $\text{PrCu}_2\text{Si}_2$ .

From a recent neutron-scattering measurement, a CF level scheme with the doublet ground state was proposed [49], as shown in Fig. 1.5. The resulting total splitting is 131K. Since the energy splitting between the first excited and the ground levels is about 15K, we do not expect the anomaly of the hyperfine coupling due to the CF splitting in the paramagnetic state.

It has been pointed out that the remarkably high  $T_N$  in  $\text{PrCu}_2\text{Si}_2$  may be due to a kind of hybridization effect [50], because the separation between the Pr ions is relatively large and the two-ion coupling is achieved by indirect interactions such as the RKKY interaction. It is an interesting question whether this hybridization effect appears in the transferred hyperfine coupling. We will discuss this problem in Sect. 4.4.

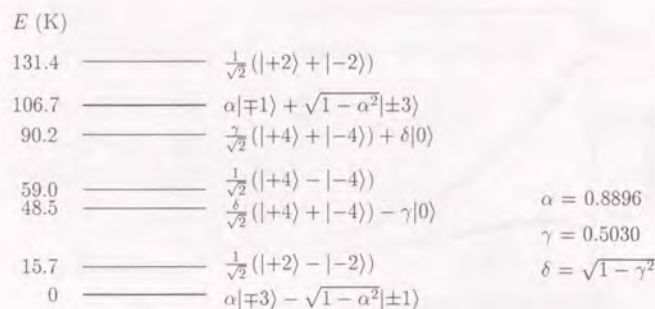


Figure 1.5. CF level scheme for  $\text{PrCu}_2\text{Si}_2$  [49].

### 1.3.6 $\text{LaCu}_2\text{Si}_2$ and $\text{YCu}_2\text{Si}_2$

The temperature dependence of magnetic susceptibilities in  $\text{LaCu}_2\text{Si}_2$  and  $\text{YCu}_2\text{Si}_2$  have not been reported so far. It was suggested that  $\text{LaCu}_2\text{Si}_2$  and  $\text{YCu}_2\text{Si}_2$  were Pauli paramagnets [51], and it was just noted that the magnetic susceptibility of  $\text{LaCu}_2\text{Si}_2$  was  $2 \times 10^{-4}$  emu/mol [35]. The Knight shift at the Si sites is independent of temperature between 77 and 500K in  $\text{LaCu}_2\text{Si}_2$  and  $\text{YCu}_2\text{Si}_2$  [52].

## 1.4 Scope of This Thesis

In investigations of the  $f$ -electron lattice system, it is important to clarify experimentally the behavior of its low-energy excitations, as well as its ground state properties. NMR is an important technique for this purpose. The final goal of the present study is to acquire enough knowledge of the transferred hyperfine field to interpret the nuclear relaxation data quantitatively. The purpose of this thesis is to clarify the mechanism of the temperature-dependent transferred hyperfine coupling, and to investigate the effect of this anomalous hyperfine coupling on the nuclear relaxation.

For these purposes, we have studied the temperature dependence of the hyperfine coupling in  $\text{CeCu}_2\text{Si}_2$  and  $\text{YbCu}_2\text{Si}_2$ . We have also studied  $\text{PrCu}_2\text{Si}_2$  to examine the CF splitting effect, and  $\text{GdCu}_2\text{Si}_2$  as a reference compound [53]. We have measured the anisotropy of the magnetic susceptibility and the Knight shifts at both Cu and Si sites, and have investigated the anisotropy and the site dependence of the hyperfine coupling in these compounds. The results of these measurements will be described in Sect. 3, and will be discussed in Sect. 4. Further, we have measured the anisotropy and the site dependence of  $T_1$  in  $\text{CeCu}_2\text{Si}_2$  and  $\text{YbCu}_2\text{Si}_2$ . These results will be given and discussed in Sect. 5.

## 2 Experimental Procedure

### 2.1 Sample Preparation

The powder samples of  $\text{CeCu}_2\text{Si}_2$ ,  $\text{YbCu}_2\text{Si}_2$  and  $\text{LaCu}_2\text{Si}_2$  were provided by Dr. J. L. Smith, Prof. Z. Fisk and Dr. D. Mandrus at Los Alamos National Laboratory. It is known that the superconducting transition temperature of  $\text{CeCu}_2\text{Si}_2$  is sensitive to the stoichiometry [54]. An effort to get a stoichiometric sample was made for the present measurement. A polycrystalline ingot of  $\text{CeCu}_2\text{Si}_2$  was prepared by arc-melting constituent elements with 0.1% excess Cu in the total weight. The weight loss was 0.1%, thus the composition is stoichiometric if all the loss is Cu. The ingot was annealed at 1100 °C for 15 days in an evacuated quartz tube and then crushed into powder. The  $\text{LaCu}_2\text{Si}_2$  sample was also synthesized by arc-melting with 0.04% excess Cu and 0.02% excess Si. The weight loss was 0.02%. Thereafter, the ingot was annealed at 1100 °C for 15 days. The prepared ingots were then crushed into powder. The powder sample of  $\text{YbCu}_2\text{Si}_2$  was cut from the same ingot as used in the previous Cu NMR measurement [12].

The samples of  $\text{PrCu}_2\text{Si}_2$  and  $\text{GdCu}_2\text{Si}_2$  were provided by Dr. E. V. Sampathkumaran at Tata Institute of Fundamental Research. They were prepared by arc-melting stoichiometric amount of constituent elements and annealed at 800 °C in evacuated quartz tubes. The ingots were then finely powdered and subsequently annealed in vacuum at the same temperature.

The sample of  $\text{YCu}_2\text{Si}_2$  was offered by Dr. S. Takagi at Tohoku University. The ingot was prepared by arc-melting stoichiometric amount of constituent elements and annealed at 1000 °C for 14 days in evacuated quartz tubes. Then the ingot was powdered for the magnetic and the NMR measurements.

### 2.2 NMR Measurements

In recent years, the magnetic alignment technique of powder samples has become familiar for NMR measurements in investigations of high- $T_C$  cuprates. This technique has improved the accuracy in the measurements of anisotropic Knight shift and anisotropic  $T_1$ .

The prepared powder samples were magnetically aligned in a magnetic field ( $H$ ) and were fixed in epoxy resin or polyethylene glycol for the NMR measurements. The alignment direction was determined from  $^{63}\text{Cu}$  NMR spectra; the  $c$ -axis lies along the alignment field ( $H_{\text{al}}$ ) in  $\text{CeCu}_2\text{Si}_2$ ,  $\text{YbCu}_2\text{Si}_2$  and  $\text{PrCu}_2\text{Si}_2$ , and it is randomly oriented in the plane perpendicular to  $H_{\text{al}}$  in  $\text{GdCu}_2\text{Si}_2$ ,  $\text{LaCu}_2\text{Si}_2$  and  $\text{YCu}_2\text{Si}_2$ . Typical  $^{63,65}\text{Cu}$  spectra with the aligned powder sample of  $\text{CeCu}_2\text{Si}_2$  are shown in Fig. 2.1. For  $\text{GdCu}_2\text{Si}_2$ , the alignment was checked also with the X-ray diffraction pattern, which showed the existence of a small fraction of misaligned particles.

The NMR measurements were carried out with phase-coherent pulse-incoherent spectrometers [55]. NMR field spectra were taken by integrating spin-echo signals with a boxcar integrator with sweeping magnetic field. For the measurements of Fourier transform frequency spectra and  $T_1$ , a digital memory was used to average the spin-echo or the free-induction signals.

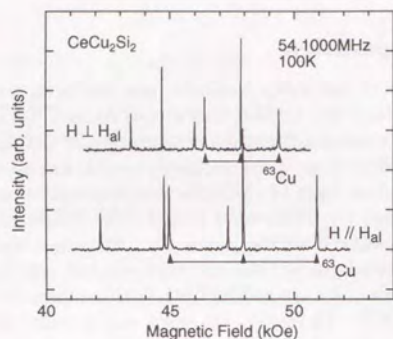


Figure 2.1. Typical  $^{63,65}\text{Cu}$  NMR field spectra in  $\text{CeCu}_2\text{Si}_2$ .

We measured  $T_1$  by observing the recovery of the spin-echo or free-induction intensity after a single saturation pulse. The nuclear magnetization recovery is described for  $^{29}\text{Si}$  ( $I = \frac{1}{2}$ ) by

$$M(t) = M(0) \{1 - C e^{-t/T_1}\}, \quad (2.1)$$

and for  $^{63}\text{Cu}$  ( $I = \frac{3}{2}$ ) by [56]

$$M(t) = M(0) \left\{ 1 - C \left[ \frac{1}{10} e^{-t/T_1} + \frac{9}{10} e^{-6t/T_1} \right] \right\} \quad (\text{for central line}), \quad (2.2)$$

$$M(t) = M(0) \left\{ 1 - C \left[ \frac{1}{10} e^{-t/T_1} + \frac{1}{2} e^{-3t/T_1} + \frac{2}{5} e^{-6t/T_1} \right] \right\} \quad (\text{for satellite line}), \quad (2.3)$$

where  $M(0)$  is the nuclear magnetization in the thermal equilibrium, and  $C$  is a parameter which describes the saturation condition.  $T_1$  was determined by fitting the data to these functions. Typical recovery curves observed in  $\text{CeCu}_2\text{Si}_2$  are shown in Fig. 2.2.

An alternating-phase pulse modulator [57] was used to the spin-echo measurements [58]. To cancel out the ringing of the receiver circuit and the sample coil after the  $\pi$  pulse, we used the sequence:

$$\begin{aligned} &(\pi/2)_x - \tau - (\pi)_x - \tau - (\text{echo})_{-x} \\ &(\pi/2)_x - \tau - (\pi)_{-x} - \tau - (\text{echo})_{-x}, \end{aligned}$$

where  $(\pi)_x$  denotes a  $\pi$  pulse along the  $x$ -axis in the rotating frame. The ringing is cancelled by adding the first and the second echoes. For the  $T_1$  measurements, we also used the sequence

$$\begin{aligned} &(\pi/2)_{-x} - \tau - (\pi)_x - \tau - (\text{echo})_x \\ &(\pi/2)_{-x} - \tau - (\pi)_{-x} - \tau - (\text{echo})_x, \end{aligned}$$

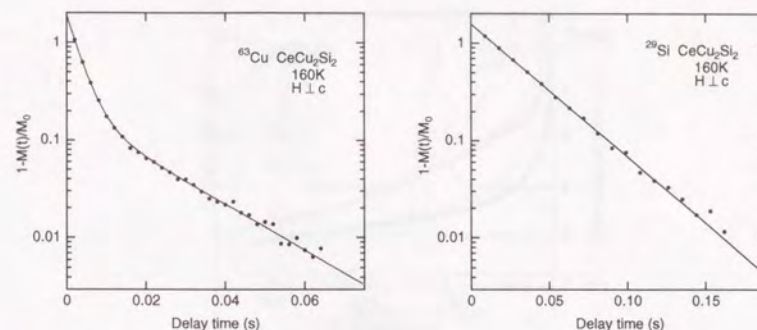


Figure 2.2. Typical recovery curves of spin-echo intensity in  $\text{CeCu}_2\text{Si}_2$ . (a) for  $^{63}\text{Cu}$ , (b) for  $^{29}\text{Si}$ . Solid lines are the theoretical curves.

where the resulting echoes are inverted in phase. Subtracting these echo signals from the signals of the former sequence makes precise zero-level correction possible.

### 2.3 Magnetic Susceptibility Measurements

A commercial SQUID magnetometer was used for the susceptibility measurements. To measure the anisotropy of the susceptibility, we prepared two cylindrical samples for each of  $\text{CeCu}_2\text{Si}_2$ ,  $\text{YbCu}_2\text{Si}_2$ ,  $\text{GdCu}_2\text{Si}_2$ , and  $\text{PrCu}_2\text{Si}_2$  with different alignment directions. The susceptibility of  $\text{LaCu}_2\text{Si}_2$  and  $\text{YCu}_2\text{Si}_2$  was measured with powder samples.

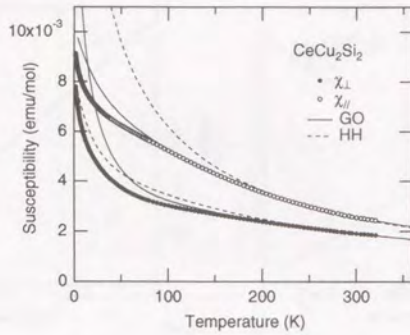


Figure 3.1. Temperature dependence of magnetic susceptibility in  $\text{CeCu}_2\text{Si}_2$ . Dashed and solid lines are the results of the molecular-field calculations for the CF level schemes in refs. [32] and [33], respectively.

### 3 Susceptibility and Knight Shift Measurements

#### 3.1 $\text{CeCu}_2\text{Si}_2$

The temperature dependence of the magnetic susceptibilities between 1.7 and 320K is shown in Fig. 3.1. Compared with previous data on single crystals [30,31], the present result is similar to that of the ‘‘Cu poor’’ sample in ref. [30].

We will give the CF analysis of the susceptibility for the  $J = \frac{5}{2}$  multiplet of the  $\text{Ce}^{3+}$  ion below. For the  $D_{4h}$  symmetry at the Ce sites, the CF Hamiltonian is

$$H_{\text{cf}} = B_2^0 O_2^0 + B_4^0 O_4^0 + B_4^4 O_4^4, \quad (3.1)$$

where  $O_i^k$  is the Stevens operators. This Hamiltonian has three doublet eigenstates; they are expressed with a single coefficient  $\eta$  as

$$|\Gamma_7^{(1)}\rangle : |\pm\frac{5}{2}\rangle \equiv \eta|\pm\frac{5}{2}\rangle + \sqrt{1-\eta^2}|\mp\frac{3}{2}\rangle, \quad (3.2)$$

$$|\Gamma_7^{(2)}\rangle : |\pm\frac{3}{2}\rangle \equiv \sqrt{1-\eta^2}|\pm\frac{5}{2}\rangle - \eta|\mp\frac{3}{2}\rangle, \quad (3.3)$$

$$|\Gamma_6\rangle : |\pm\frac{7}{2}\rangle \equiv |\pm\frac{1}{2}\rangle. \quad (3.4)$$

The single site susceptibility is generally given by

$$\chi_{\alpha}^{\text{ss}} = \frac{g_J^2 \mu_B^2}{Z} \sum_{\Gamma_i m_i} [\beta e^{-\beta E_{\Gamma_i}} \sum_{m'_i} |\langle \Gamma_i m_i | J_{\alpha} | \Gamma_i m'_i \rangle|^2]$$

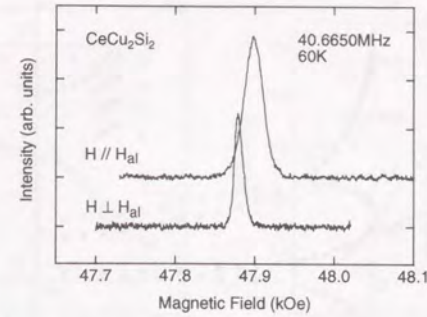


Figure 3.2.  $^{29}\text{Si}$  NMR field spectra at 60K in  $\text{CeCu}_2\text{Si}_2$ .

$$+ \sum_{\Gamma_j m_j} \frac{e^{-\beta E_{\Gamma_i}} - e^{-\beta E_{\Gamma_j}}}{E_{\Gamma_j} - E_{\Gamma_i}} |\langle \Gamma_i m_i | J_{\alpha} | \Gamma_j m_j \rangle|^2 \quad (\alpha = x, y, z), \quad (3.5)$$

where  $|\Gamma_i m_i\rangle$  represents a CF state with the  $\Gamma_i$  symmetry and  $\beta = 1/k_B T$ . For  $\text{CeCu}_2\text{Si}_2$ , two different CF level schemes were proposed from the inelastic neutron-scattering measurements. Both the level schemes have the ground-state doublet  $\Gamma_7^{(1)}$  and the first-excited-state doublet  $\Gamma_6$ , as shown in Fig. 1.3. For this level scheme we obtain the single site susceptibilities

$$\chi_{\parallel}^{\text{ss}} = \frac{g_J^2 \mu_B^2}{Z} \left\{ \beta \left[ 2 \left( \frac{3}{2} - 4\eta^2 \right)^2 + \frac{1}{2} e^{-\beta \Delta_1} + 2 \left( \frac{5}{2} - 4\eta^2 \right)^2 e^{-\beta \Delta_2} \right] + 64\eta^2 (1 - \eta^2) \frac{1 - e^{-\beta \Delta_2}}{\Delta_2} \right\} \quad (3.6)$$

and

$$\chi_{\perp}^{\text{ss}} = \frac{g_J^2 \mu_B^2}{Z} \left\{ \beta \left[ 10\eta^2 (1 - \eta^2) (1 + e^{-\beta \Delta_2}) + \frac{9}{2} e^{-\beta \Delta_1} \right] + 8\eta^2 \frac{e^{-\beta \Delta_1} - e^{-\beta \Delta_2}}{\Delta_2 - \Delta_1} + 8(1 - \eta^2) \frac{1 - e^{-\beta \Delta_1}}{\Delta_1} + 5(1 - 2\eta^2)^2 \frac{1 - e^{-\beta \Delta_2}}{\Delta_2} \right\}, \quad (3.7)$$

where  $\Delta_1 = E_{\Gamma_6} - E_{\Gamma_7^{(1)}}$  and  $\Delta_2 = E_{\Gamma_7^{(2)}} - E_{\Gamma_7^{(1)}}$ . The results of the molecular-field calculation

$$\chi_{\alpha} = \frac{\chi_{\alpha}^{\text{ss}}}{1 - \lambda_{\alpha} \chi_{\alpha}^{\text{ss}}} \quad (3.8)$$

are shown in Fig. 3.1. The anisotropic molecular-field parameters,  $\lambda_{\parallel} = -28\text{mol/emu}$  and  $\lambda_{\perp} = -118\text{mol/emu}$  for the HH model ( $\eta = 0.83$ ), and  $\lambda_{\parallel} = -97\text{mol/emu}$  and

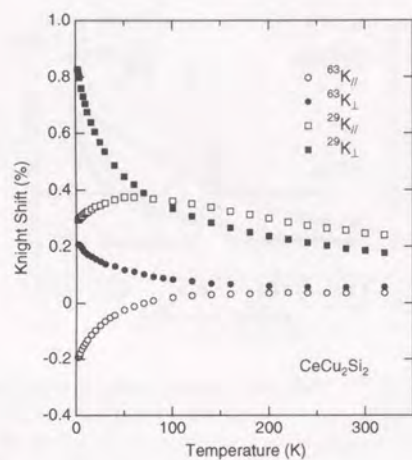


Figure 3.3. Temperature dependence of Knight shifts at Cu and Si sites in  $\text{CeCu}_2\text{Si}_2$ .

$\lambda_{\perp} = -58\text{mol}/\text{emu}$  for the GO model ( $\eta = 0.88$ ), were determined so as to give the best fit above 200K. Within this CF calculation, the GO model reproduces the measured susceptibilities better.

The principal values of the Knight shift ( $K_{\parallel}$  and  $K_{\perp}$ ) at the Cu and Si sites were determined between 2 and 320K from the  $^{63}\text{Cu}$  and  $^{29}\text{Si}$  spin-echo spectra, where  $K_{\parallel}$  and  $K_{\perp}$  denote the components along the  $c$ -axis and in the basal plane, respectively. It is found from the  $^{63}\text{Cu}$  spectra (Fig. 2.1) that fairly good alignment was achieved in this sample. Figure 3.2 shows typical  $^{29}\text{Si}$  spectra. The values of  $^{29}K_{\parallel}$  and  $^{29}K_{\perp}$  were determined with the spectrum peak. The value of  $^{63}K_{\parallel}$  was determined with the central line, while  $^{63}K_{\perp}$  was determined with the central line with the quadrupolar correction [59] using the quadrupole frequency obtained from the satellite lines.

The temperature dependence of the Knight shifts is shown in Fig. 3.3. Similar data below about 100K were previously reported [36,37]. The observed temperature dependence is remarkably different from that of the susceptibilities. To clarify the difference, the Knight shifts at the Cu and Si sites are plotted against the susceptibilities in Figs. 3.4 (a) and 3.4 (b), respectively. These  $K-\chi$  plots clearly show that the transferred hyperfine coupling is temperature-dependent in  $\text{CeCu}_2\text{Si}_2$ . Since the susceptibilities and the Knight shifts were measured under the different magnetic fields, the observed temperature dependence might be due to the nonlinearity of the magnetization curve. However, we measured the magnetization curve at 4.2K, and it was found that the difference be-

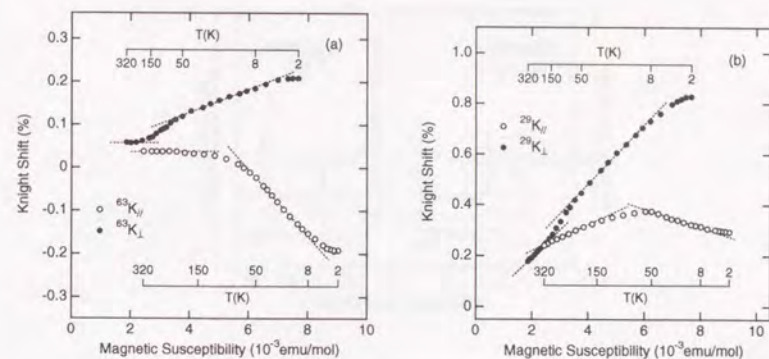


Figure 3.4.  $K-\chi$  plots for (a) Cu sites and (b) Si sites in  $\text{CeCu}_2\text{Si}_2$ . Dashed lines are linear fitting results.

(kOe/ $\mu_B$ )	$^{63}A_{\parallel}$	$^{63}A_{\perp}$	$^{29}A_{\parallel}$	$^{29}A_{\perp}$
10 ~ 50K	-4.2	1.5	-1.9	6.4
200K ~	0.1	0.0	2.9	6.0

Table 3.1. Hyperfine coupling constants in  $\text{CeCu}_2\text{Si}_2$ .

tween the susceptibilities at 10 and 50kOe is about 1%. Thus the nonlinear effect of the magnetization curves is negligible.

One of the most important findings is that the observed temperature dependences of the Knight shifts at both the sites are obviously different. This indicates that the observed site dependence of the Knight shifts cannot be explained by the difference in the hyperfine coupling between the conduction electrons and the ligand nuclei.

The  $K-\chi$  plots for both the sites are almost linear in common in the temperature ranges between about 10 and 50K and above about 200K. The hyperfine couplings defined as the slope of the  $K-\chi$  plots for these temperature ranges are given in Table 3.1. The anisotropy of the hyperfine couplings increases at low temperatures. It should be noticed that the signs of the hyperfine coupling along the  $c$ -axis are negative at the low temperatures. This sign is anomalous because the experimentally observed hyperfine coupling is almost always positive in other Ce compounds.

Since  $T_K$  in  $\text{CeCu}_2\text{Si}_2$  is about 10K, the change in the hyperfine coupling around 100K is most likely attributed to the CF splitting. The nonlinearity in the  $K-\chi$  plots is ob-

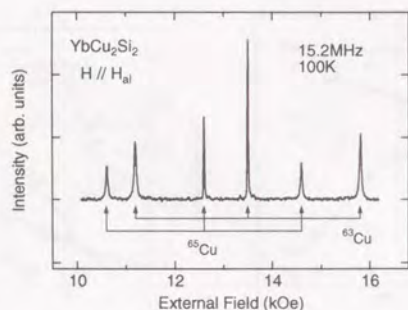


Figure 3.5. Typical  $^{63,65}\text{Cu}$  NMR field spectrum for  $H \parallel H_{ai}$  in  $\text{YbCu}_2\text{Si}_2$ .

served also below about 10K, where the Knight shifts are weakly temperature-dependent, while the magnetic susceptibilities continue to increase as decreasing temperature. This nonlinearity is the opposite direction to the previous result [35]; they reported the enhancement of the hyperfine coupling. We did not correct the measured susceptibilities for an impurity contribution, because there is no convincing reason to consider the "Curie tail" as the impurity effect. Of course it cannot be denied that the anomaly is due to the impurity contribution to the susceptibility. However, the Knight shifts have weaker temperature dependence below 5K than at higher temperatures, thus we conclude the absence of the enhancement.

### 3.2 $\text{YbCu}_2\text{Si}_2$

Figure 3.5 shows a typical  $^{63,65}\text{Cu}$  spectrum in  $\text{YbCu}_2\text{Si}_2$ , which indicates a good alignment of this sample. Typical Si spectra are shown in Fig. 3.6. We obtained  $^{29}K_{\parallel}$  and  $^{29}K_{\perp}$  from the spectrum peak position. The results are shown in Fig. 3.7, with the previous data for  $^{63}K_{\parallel}$  and  $^{63}K_{\perp}$  [12].

These  $^{29}\text{Si}$  Knight shifts were measured under a higher external field than for the previous data of  $^{63}K_{\parallel}$  and  $^{63}K_{\perp}$ . To examine the field dependence of the Knight shifts, we also measured  $^{63}K_{\parallel}$  under  $H \sim 50\text{kOe}$ ; the result is shown in Fig. 3.7.  $^{63}K_{\parallel}$  was determined from the peak position of the central line. The result agrees well to the low-field data, thus we can neglect the field dependence.

The Knight shifts at the Cu and Si sites are plotted against the magnetic susceptibilities (Fig. 1.4) [12] in Figs. 3.8 (a) and 3.8 (b). These  $K-\chi$  plots clearly show that the hyperfine coupling at the Si sites is temperature-dependent, as well as at the Cu sites. Further, the difference between  $^{29}K_{\perp}$  and  $^{63}K_{\perp}$  is remarkable at the low temperatures. The Knight shifts are almost linear to the susceptibilities above about 100K. The

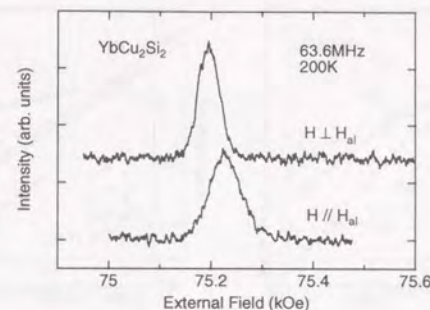


Figure 3.6. Typical  $^{29}\text{Si}$  NMR field spectra in  $\text{YbCu}_2\text{Si}_2$ .

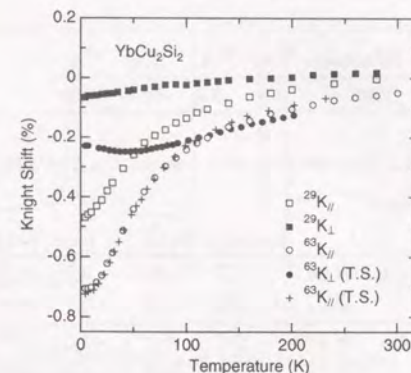


Figure 3.7. Temperature dependence of Knight shifts at Si and Cu sites in  $\text{YbCu}_2\text{Si}_2$ . The data of  $^{63}K_{\parallel}$  and  $^{63}K_{\perp}$  by Shimizu *et al.* [12] are also shown.

hyperfine couplings deduced from the data above 120K are shown in Table 3.2.

There are some common features in the temperature-dependent hyperfine coupling observed in  $\text{CeCu}_2\text{Si}_2$  and  $\text{YbCu}_2\text{Si}_2$ . First, the temperature dependences at the Cu and Si sites are different. Next, the anisotropy increases at low temperatures. We will discuss these points in the next section.

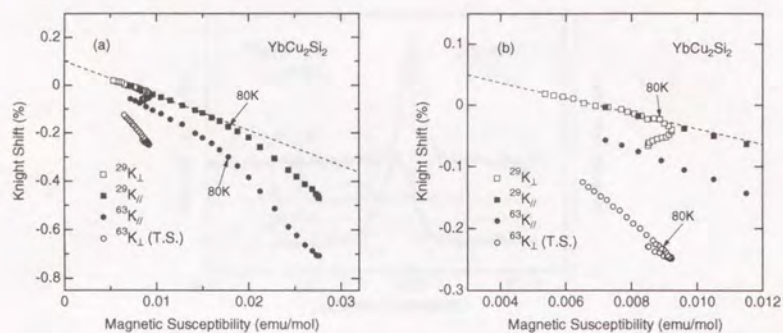


Figure 3.8. (a)  $K-\chi$  plots for  $\text{YbCu}_2\text{Si}_2$ . (b) enlarged for  $^{29}\text{K}_{\parallel}$  and  $^{29}\text{K}_{\perp}$ . Dashed line is the linear fitting result for  $^{29}\text{K}_{\perp}$ .

(kOe/ $\mu_B$ )	$^{63}A_{\parallel}$	$^{63}A_{\perp}$	$^{29}A_{\parallel}$	$^{29}A_{\perp}$
120K ~	-1.1	-2.4	-0.78	-0.69

Table 3.2. Hyperfine coupling constants in  $\text{YbCu}_2\text{Si}_2$ .

	$\mu_{\text{eff}}(\mu_B)$	$\Theta(\text{K})$	$\chi_0$ (emu/mol)
$\text{GdCu}_2\text{Si}_2$ $H \parallel c$	7.7	-21	$4.3 \times 10^{-4}$
$H \perp c$	7.9	-19	$0.7 \times 10^{-4}$
$\text{PrCu}_2\text{Si}_2$ $H \parallel c$	3.7	6.5	$-3.5 \times 10^{-4}$
$H \perp c$	3.7	-12.9	$-3.5 \times 10^{-4}$

Table 3.3. Parameters obtained from the magnetic susceptibilities of  $\text{GdCu}_2\text{Si}_2$  and  $\text{PrCu}_2\text{Si}_2$ .

### 3.3 $\text{GdCu}_2\text{Si}_2$

The magnetic susceptibility was measured between 5 and 310K in a magnetic field of 5kOe. The measured susceptibility for  $H \parallel H_{\text{al}}$  corresponds to  $\chi_{\perp}$ , and that for  $H \perp H_{\text{al}}$  is the average of  $\chi_{\parallel}$  and  $\chi_{\perp}$ . We thus deduced  $\chi_{\parallel}$  using this relation. The temperature dependence of  $\chi_{\perp}$  and  $\chi_{\parallel}$  is shown in Figs. 3.9 (a) and 3.9 (b). This result is consistent

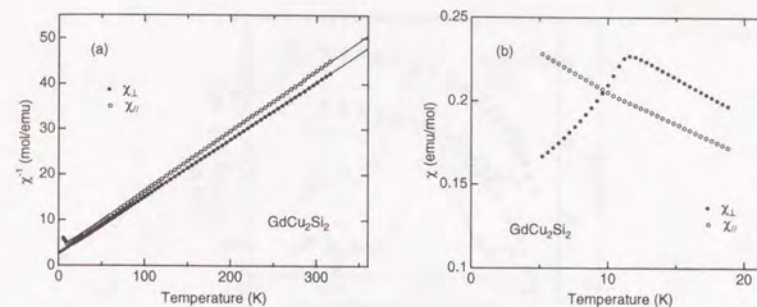


Figure 3.9. Temperature dependence of magnetic susceptibility in  $\text{GdCu}_2\text{Si}_2$ . (a) inverse susceptibility, (b) low temperature susceptibility.

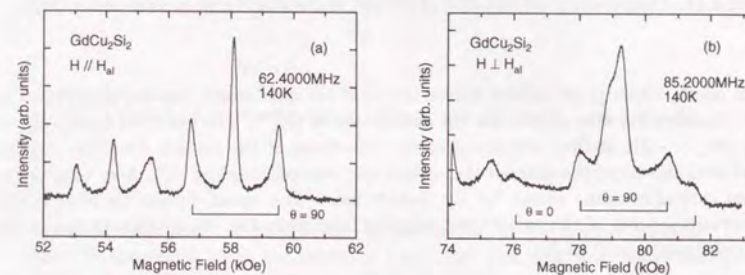


Figure 3.10.  $^{63}\text{Cu}$  NMR field spectra at 140K in  $\text{GdCu}_2\text{Si}_2$ . (a) for  $H \parallel H_{\text{al}}$ , and (b)  $H \perp H_{\text{al}}$ .  $^{63}\text{Cu}$  satellites are shown with arrows.

with the previous measurement on the powder sample [46]. In the paramagnetic state, the anisotropy is small and both  $\chi_{\perp}$  and  $\chi_{\parallel}$  can be fitted with a modified Curie-Weiss formula

$$\chi(T) = \frac{C}{(T - \Theta)} + \chi_0. \quad (3.9)$$

The deduced parameters from the fitting above 40K are listed in Table 3.3. The effective moments  $\mu_{\text{eff}}$  are near the free  $\text{Gd}^{3+}$  value of  $7.94\mu_B$ .

There is only a small anisotropy in the values of  $\Theta$ . In general, the anisotropy of the Weiss temperature in intermetallic compounds with localized  $4f$  moments is due to both

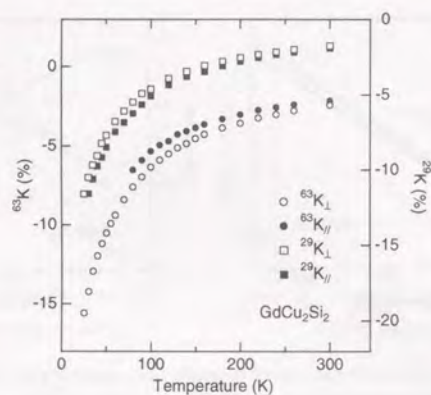


Figure 3.11. Temperature dependence of Knight shifts at Cu and Si sites in  $\text{GdCu}_2\text{Si}_2$ .

the CF effect, which gives one-ion anisotropy, and the anisotropic two-ion coupling. The former contribution is negligible for the  $S$ -state ion of  $\text{Gd}^{3+}$ . The observed anisotropy of  $\Theta$ ,  $\Theta_{\parallel} - \Theta_{\perp} \sim -2\text{K}$ , is thus attributed to the anisotropy of the two-ion coupling. Among several mechanisms responsible for the anisotropic two-ion coupling [60], those originating from an orbital moment vanish for the  $S$ -state ions. The direct dipolar coupling is one of important sources of the anisotropic coupling, and gives the Weiss temperature in the high temperature limit as [61]

$$\Theta = \frac{g_j^2 \mu_B^2 J(J+1)}{3k_B} \sum_i \frac{1 - 3\cos^2 \theta_{ij}}{r_{ij}^3}, \quad (3.10)$$

where  $r_{ij}$  is the radius vector connecting atoms  $i$  and  $j$ , and  $\theta_{ij}$  is the angle between the external field and  $r_{ij}$ . The calculated contribution for  $\text{GdCu}_2\text{Si}_2$  is  $\Theta_{\parallel} - \Theta_{\perp} \sim -1.0\text{K}$ , which is comparable to the observed value. This agreement indicates that the anisotropy of the two-ion coupling is attributed to the direct dipolar interaction and that the indirect interaction is essentially isotropic. Thus we may suspect that the conduction electron polarization is also isotropic. Therefore this Gd compound can serve as a good reference system for the  $\text{RCu}_2\text{Si}_2$  series with the isotropic  $s$ - $f$  exchange interaction.

The Knight shift  $K_{\parallel}$  and  $K_{\perp}$  at the Cu and Si sites were determined from  $^{63}\text{Cu}$  and  $^{29}\text{Si}$  spin-echo spectra. Figures 3.10 (a) and 3.10 (b) show typical  $^{63}\text{Cu}$  spectra for  $H \parallel H_{\text{al}}$  and  $H \perp H_{\text{al}}$ , respectively. The values of  $^{63}K_{\parallel}$  and  $^{63}K_{\perp}$  were determined with the satellite singularities for  $\theta = 0^\circ$  and  $90^\circ$ , respectively, where  $\theta$  is the angle between the magnetic field and the  $c$ -axis. The temperature dependence of  $^{63}K_{\parallel}$  and  $^{63}K_{\perp}$  is shown in Fig. 3.11. The value of  $^{63}K_{\parallel}$  could not be determined below 80K, because spectral broadening was

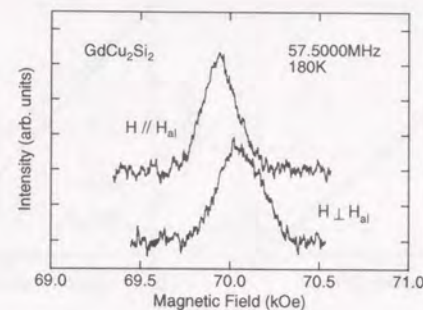


Figure 3.12.  $^{29}\text{Si}$  NMR field spectra at 180K in  $\text{GdCu}_2\text{Si}_2$ .

(kOe/ $\mu_B$ )	$^{63}A_{\parallel}$	$^{63}A_{\perp}$	$^{29}A_{\parallel}$	$^{29}A_{\perp}$
$\text{GdCu}_2\text{Si}_2$	-5.0	-5.1	-4.7	-3.8
$\text{PrCu}_2\text{Si}_2$	2.5	1.4	3.7	3.7

Table 3.4. Hyperfine coupling constants in  $\text{GdCu}_2\text{Si}_2$  and  $\text{PrCu}_2\text{Si}_2$ .

too severe to determine the singularities in the spectra at low temperatures.

The  $^{29}\text{Si}$  spectra at 180K are shown in Fig. 3.12. The peak position of the spectrum for  $H \parallel H_{\text{al}}$  gives  $^{29}K_{\perp}$ . On the other hand, the peak position of the spectrum for  $H \perp H_{\text{al}}$  corresponds to the average of  $^{29}K_{\perp}$  and  $^{29}K_{\parallel}$ . Thus  $^{29}K_{\parallel}$  was obtained from  $^{29}K_{\perp}$  and this average value. The temperature dependence of  $^{29}K_{\perp}$  and  $^{29}K_{\parallel}$  is also shown in Fig. 3.11.

The Knight shifts at both the Cu and Si sites exhibit a similar temperature dependence to the magnetic susceptibility. Since these Knight shifts were measured under the magnetic field of about 70kOe, they are plotted against the susceptibility measured at 70kOe in Figs. 3.13 (a) and 3.13 (b). As can be seen, good linear relations were obtained. The hyperfine coupling constants are determined as the slope of these  $K$ - $\chi$  plots and the results are given in Table 3.4.

### 3.4 $\text{PrCu}_2\text{Si}_2$

Figures 3.14 (a) and 3.14 (b) present the temperature dependence of the susceptibility in  $\text{PrCu}_2\text{Si}_2$ , which was measured under the magnetic field of 5kOe. Above  $T_N$ , both  $\chi_{\perp}$  and  $\chi_{\parallel}$  follow the Curie-Weiss formula eq. (3.9), although a small deviation occurs below about 80K in  $\chi_{\perp}$ . Since the total CF splitting is about 130K [49], this deviation is

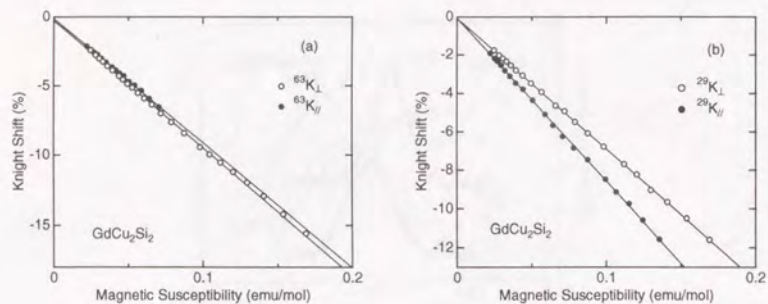


Figure 3.13. Knight shifts are plotted against the susceptibility. (a) for Cu sites, (b) for Si sites. Solid lines are the linear fitting results.

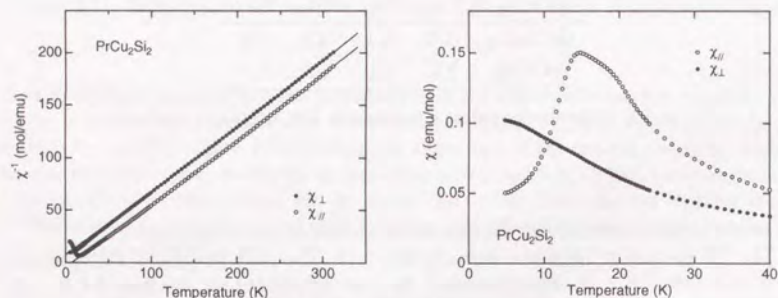


Figure 3.14. Temperature dependence of magnetic susceptibility in  $\text{PrCu}_2\text{Si}_2$ . (a) inverse susceptibility, (b) low temperature susceptibility.

reasonably due to the CF effect. The results of the fitting to eq. (3.9) above 150K are also listed in Table 3.3. The obtained values of  $\mu_{\text{eff}}$  are slightly larger than the free  $\text{Pr}^{3+}$  value of  $3.58\mu_B$ . In contrast to the results for  $\text{GdCu}_2\text{Si}_2$ , the anisotropy of  $\Theta$  is significant in  $\text{PrCu}_2\text{Si}_2$ . At low temperatures, anomalies are found at 13K and 20K in  $\chi_{\parallel}$ . Remarkable decrease in  $\chi_{\parallel}$  is observed below 13K rather than just below  $T_N$ .

Figures 3.15 and 3.16 show typical  $^{63,65}\text{Cu}$  and  $^{29}\text{Si}$  spectra, respectively. The Knight shifts at the Cu sites were determined with the satellite singularities, as in  $\text{GdCu}_2\text{Si}_2$ . The Knight shifts at the Si sites were determined with the peak position in the spectra.

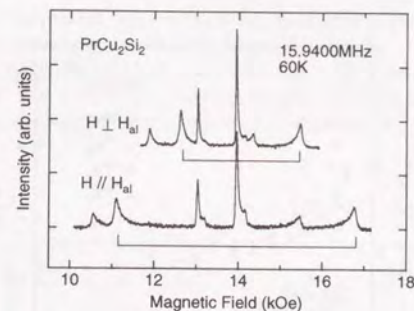


Figure 3.15. Typical  $^{63}\text{Cu}$  NMR field spectra in  $\text{PrCu}_2\text{Si}_2$ .

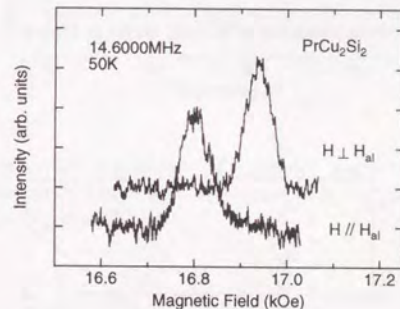


Figure 3.16. Typical  $^{29}\text{Si}$  NMR field spectra in  $\text{PrCu}_2\text{Si}_2$ .

The resulting temperature dependence is given in Fig. 3.17.

The  $K$ - $\chi$  plots for  $\text{PrCu}_2\text{Si}_2$  are presented in Fig. 3.18, where the linear relation between the Knight shift and the susceptibility is satisfied except for below 40K. The hyperfine coupling constants for the Cu and Si sites, deduced from the data above 40K, are listed in Table 3.4. It is found that the anisotropy and the site dependence are different from those in  $\text{GdCu}_2\text{Si}_2$ .

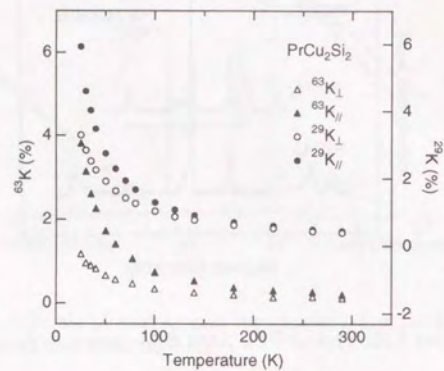


Figure 3.17. Temperature dependence of Knight shifts at Cu and Si sites in  $\text{PrCu}_2\text{Si}_2$ .

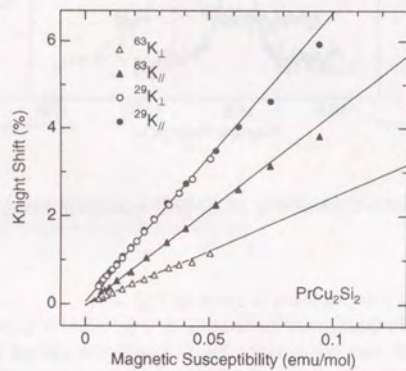


Figure 3.18. Knight shifts at Cu and Si sites in  $\text{PrCu}_2\text{Si}_2$  are plotted against magnetic susceptibility.

### 3.5 $\text{YCu}_2\text{Si}_2$ and $\text{LaCu}_2\text{Si}_2$

In this subsection, we present the results of the susceptibility and the nuclear relaxation measurements on reference compounds,  $\text{YCu}_2\text{Si}_2$  and  $\text{LaCu}_2\text{Si}_2$ .

The magnetic susceptibilities of  $\text{YCu}_2\text{Si}_2$  and  $\text{LaCu}_2\text{Si}_2$  measured with the powder samples are shown in Fig. 3.19. The observed temperature-independent susceptibilities are dominated by the diamagnetic contributions of the ion cores [62], and the Pauli para-

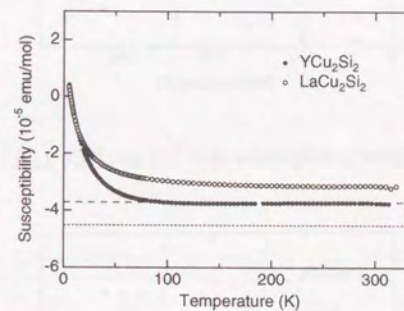


Figure 3.19. Temperature dependence of magnetic susceptibility in  $\text{YCu}_2\text{Si}_2$  and  $\text{LaCu}_2\text{Si}_2$ . Dashed and dotted lines are the diamagnetic contributions of the ion cores for  $\text{YCu}_2\text{Si}_2$  and  $\text{LaCu}_2\text{Si}_2$ , respectively.

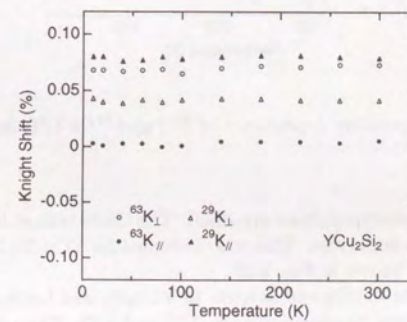


Figure 3.20. Temperature dependence of Knight shift in  $\text{YCu}_2\text{Si}_2$ .

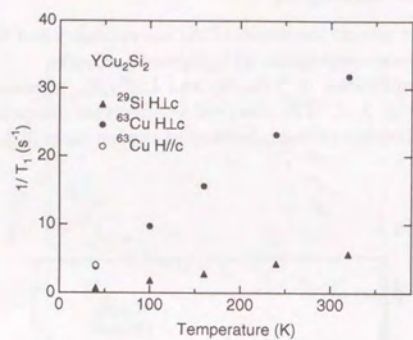


Figure 3.21. Temperature dependence of <sup>29</sup>Si and <sup>63</sup>Cu 1/T<sub>1</sub> in YCu<sub>2</sub>Si<sub>2</sub>.

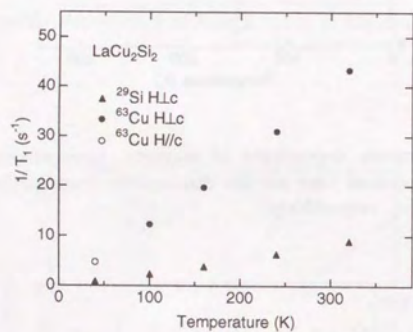


Figure 3.22. Temperature dependence of <sup>29</sup>Si and <sup>63</sup>Cu 1/T<sub>1</sub> in LaCu<sub>2</sub>Si<sub>2</sub>.

magnetic and the orbital susceptibilities are small. The Curie tails at low temperatures is probably due to magnetic impurities. This was confirmed for YCu<sub>2</sub>Si<sub>2</sub> by the temperature independent Knight shift shown in Fig. 3.20.

We also measured  $T_1$  at the Cu and Si sites. In YCu<sub>2</sub>Si<sub>2</sub> and LaCu<sub>2</sub>Si<sub>2</sub>,  $1/T_1$  is almost proportional to temperature, as shown in Figs. 3.21 and 3.22. The anisotropy at the Cu sites is very small. The obtained values of  $1/T_1 T$  below 100K are listed in Table 3.5. These observations indicate that these compounds behave as a simple paramagnetic metal.

(s <sup>-1</sup> K <sup>-1</sup> )	<sup>29</sup> Si (H ⊥ c)	<sup>63</sup> Cu (H ⊥ c)	<sup>63</sup> Cu (H    c)
YCu <sub>2</sub> Si <sub>2</sub>	0.018	0.097	0.102
LaCu <sub>2</sub> Si <sub>2</sub>	0.022	0.120	0.120

Table 3.5.  $1/T_1 T$  in YCu<sub>2</sub>Si<sub>2</sub> and LaCu<sub>2</sub>Si<sub>2</sub>.

## 4 Discussion on Static Measurements

### 4.1 Transferred Hyperfine Coupling in GdCu<sub>2</sub>Si<sub>2</sub>

In this subsection, we discuss the anisotropy and the site dependence of the transferred hyperfine coupling in the reference compound GdCu<sub>2</sub>Si<sub>2</sub>, where the "normal" linear  $K - \chi$  plots were obtained.

If the conduction electron band structure of GdCu<sub>2</sub>Si<sub>2</sub> is not remarkably different from that of the paramagnetic metals YCu<sub>2</sub>Si<sub>2</sub> and LaCu<sub>2</sub>Si<sub>2</sub>, the hyperfine coupling between the conduction electrons and the Cu or Si nuclei in GdCu<sub>2</sub>Si<sub>2</sub> is the same as the hyperfine coupling that causes the Knight shifts and the nuclear relaxations in YCu<sub>2</sub>Si<sub>2</sub> and LaCu<sub>2</sub>Si<sub>2</sub>. Let us examine the experimental results from this point of view.

In LaCu<sub>2</sub>Si<sub>2</sub> and YCu<sub>2</sub>Si<sub>2</sub>, the temperature-independent Knight shifts were observed, but we cannot extract the spin contribution from the observed Knight shift. Thus we cannot estimate the hyperfine coupling  $A_c$  in YCu<sub>2</sub>Si<sub>2</sub> and LaCu<sub>2</sub>Si<sub>2</sub>. We instead estimate it from  $T_1$ . The relaxation rates are written as

$$\begin{aligned} \left(\frac{1}{T_1 T}\right)_{H\parallel c} &\propto \gamma^2 A_{c\perp}^2 \sum_q \frac{\chi''(q, \omega_N)}{\omega_N}, \\ \left(\frac{1}{T_1 T}\right)_{H\perp c} &\propto \gamma^2 \frac{A_{c\perp}^2 + A_{c\parallel}^2}{2} \sum_q \frac{\chi''(q, \omega_N)}{\omega_N}, \end{aligned} \quad (4.1)$$

where the  $q$  dependence of  $A_c$  and the anisotropy of the dynamical susceptibility were neglected. These are good approximations in normal metals. According to eq. (1.7), if the  $s$ - $f$  exchange interaction is isotropic, the ratio  $A_{c\parallel}/A_{c\perp}$  is equal to the hyperfine coupling ratio  $A_{\parallel}/A_{\perp}$  in GdCu<sub>2</sub>Si<sub>2</sub>. Then we can write a ratio as

$$\left(\frac{1}{T_1 T}\right)_{H\perp c} / \left(\frac{1}{T_1 T}\right)_{H\parallel c} = \frac{A_{\perp}^2 + A_{\parallel}^2}{2A_{\perp}^2}. \quad (4.2)$$

Since the hyperfine coupling in GdCu<sub>2</sub>Si<sub>2</sub> and  $1/T_1$  in YCu<sub>2</sub>Si<sub>2</sub> and LaCu<sub>2</sub>Si<sub>2</sub> are almost isotropic, this relation is well satisfied for the Cu sites.

On the other hand, the ratio between  $A_c$  at the Cu and Si sites is equal to the hyperfine coupling ratio in GdCu<sub>2</sub>Si<sub>2</sub> according to eq. (1.7). Then the relaxation rate ratio between the Cu and Si sites can be written as

$${}^{29}\left(\frac{1}{T_1 T}\right)_{H\perp c} / {}^{63}\left(\frac{1}{T_1 T}\right)_{H\perp c} = \left(\frac{{}^{29}\gamma_N}{{}^{63}\gamma_N}\right)^2 \frac{{}^{29}A_{\parallel}^2 + {}^{29}A_{\perp}^2}{{}^{63}A_{\parallel}^2 + {}^{63}A_{\perp}^2}. \quad (4.3)$$

We obtain the experimental results 0.19 for YCu<sub>2</sub>Si<sub>2</sub> and 0.18 for LaCu<sub>2</sub>Si<sub>2</sub> from the  $T_1$  results, while we obtain 0.40 from the hyperfine coupling in GdCu<sub>2</sub>Si<sub>2</sub>. This disagreement indicates that the hyperfine coupling in GdCu<sub>2</sub>Si<sub>2</sub> cannot be written as eq. (1.7). This is partly due to the  $G \neq 0$  term neglected in eq. (1.7).

### 4.2 Sign of Transferred Hyperfine Coupling

In the following subsections, we will discuss the mechanism of the temperature-dependent transferred hyperfine coupling.

At first we consider the experimental fact in rare-earth intermetallics that the hyperfine coupling at the ligand sites is positive for rare-earth ions with  $J = L - S$  and negative for  $J = L + S$ . This rule has been valid regardless of the ligand atoms and the crystal structures. In general, the hyperfine coupling of the  $p$  and  $d$  orbitals is mainly due to the core polarization, and its sign and magnitude change depending on the orbitals [9, 63]. Therefore, the empirical rule strongly indicates that the transferred hyperfine coupling in the rare-earth intermetallics is dominated by the spin polarization of the  $s$  orbital in the ligand atoms.

Then what is the mechanism of the  $s$  spin polarization responsible for the empirical rule? There are a few theoretical studies on the transferred hyperfine coupling in rare-earth compounds. The unrestricted Hartree-Fock calculation for GdF<sub>3</sub> revealed that the covalency and overlap between the F  $2s$  orbital and the Gd  $5s$  and  $5p$  closed shells give the dominant contribution and the correct sign, and further that the  $4f$  overlap contribution is very small and opposite in sign [22]. As for Gd metal, it was argued that the  $5s$  and  $5p$  components of the conduction electrons are important for the exchange interaction between the  $4f$  and the conduction electrons [18]. Since the  $4f$  orbital lies inside the  $5s$  and  $5p$  orbitals, it is plausible that the spin polarizations of these outer shell orbitals give the main contribution to the transferred hyperfine coupling in Gd intermetallics. The polarization of the outer closed shells is due to the intraatomic exchange, thus its sign is possibly independent of the crystal structures and the ligand atoms. The invariant sign of the transferred hyperfine coupling for other rare-earth elements suggests that this process is also dominant there.

This is the most likely origin of the empirical rule. As for the  $4f$  covalency contribution, it could reverse its sign depending on the  $4f$  wave functions and the ligand atom position as shown below, thus it is not appropriate for the origin. It should be mentioned that the rule is obeyed even in Ce mononitrides [65], where the strong  $f$ -ligand  $p$  hybridization affects their physical properties [23].

### 4.3 Temperature-Dependent Hyperfine Coupling in CeCu<sub>2</sub>Si<sub>2</sub> and YbCu<sub>2</sub>Si<sub>2</sub>

We now turn to discuss the temperature-dependent transferred hyperfine coupling in CeCu<sub>2</sub>Si<sub>2</sub> and YbCu<sub>2</sub>Si<sub>2</sub>. This hyperfine coupling can be characterized by the site dependence and the strong anisotropy at low temperatures. With regard to the discussion in the previous subsection, the negative hyperfine couplings for  ${}^{63}K_{\parallel}$  and  ${}^{29}K_{\parallel}$  at low temperatures in CeCu<sub>2</sub>Si<sub>2</sub> are exceptions to the rule. To our knowledge, this is the only case in the rare-earth intermetallics. When the contribution of the  $p$  or  $d$  orbitals in the ligand atom exceeds that of the  $s$  orbital, the rule can be violated. However, this is unlikely, because the hyperfine coupling of the  $s$  orbitals is much larger than that of the other orbitals. Therefore it is reasonably expected that the direct  $4f$ -ligand  $s$  hybridization is responsible for these exceptions. It should be pointed out here that the

rule is valid also for almost all actinide intermetallics but the exceptions were observed at the Pt sites in UPt<sub>3</sub> [66] and at the Cu sites in U<sub>3</sub>Cu<sub>3</sub>Sn<sub>4</sub> [67]. Since the 5*f* orbital in U atoms has larger extent than the 4*f* orbital, it is expected that the direct *f*-ligand hybridization is often significant in uranium intermetallics.

It is often argued that the hyperfine coupling involving the ligand *s* orbital is isotropic, but this is not always valid as shown below. It is not necessary to consider the non-*s* contribution to explain the observed large anisotropy. We consider the anisotropy and the temperature dependence of the transferred hyperfine coupling caused by the *f*-ligand *s* hybridization for the 4*f*<sup>1</sup> configuration. The expression of the induced spin polarization at the ligand orbital has been given for YbP [14] and CeP [68] with a cubic structure. Taking account of the anisotropy, the induced spin polarization is

$$\begin{aligned} \langle \sigma_\alpha \rangle = & -\frac{g_J \mu_B H}{Z} \sum_n \sum_{\Gamma, m_i} [\beta e^{-\beta E_{\Gamma_i}} \sum_{m'_i} \langle n\Gamma_i m_i | J_{n\alpha} | n\Gamma_i m'_i \rangle \langle n\Gamma_i m'_i | \sigma_\alpha | n\Gamma_i m_i \rangle \\ & + \sum_{\Gamma_j m_j} \frac{e^{-\beta E_{\Gamma_i}} - e^{-\beta E_{\Gamma_j}}}{E_{\Gamma_j} - E_{\Gamma_i}} \langle n\Gamma_i m_i | J_{n\alpha} | n\Gamma_j m_j \rangle \langle n\Gamma_j m_j | \sigma_\alpha | n\Gamma_i m_i \rangle] \\ & (\alpha = x, y, z), \end{aligned} \quad (4.4)$$

where  $\sigma_\alpha$  is a spin operator of the ligand *s* orbital, and  $|n\Gamma_i m_i\rangle$  is a CF state of the *n*th Ce ion. This spin polarization has a form where each of the Curie and the Van Vleck terms in the single ion susceptibility eq. (3.5) has a distinct hyperfine coupling constant. We here define the spin and the mixing matrix elements for the processes 4*f*<sup>1</sup> → 4*f*<sup>0</sup>*L* as

$$\langle n\Gamma_j m_j | \sigma_\alpha | n\Gamma_i m_i \rangle \equiv \sum_{\sigma_L \sigma'_L} \frac{\langle \sigma_L | \sigma_\alpha | \sigma'_L \rangle \langle \sigma_L | V | n\Gamma_j m_j \rangle^* \langle \sigma'_L | V | n\Gamma_i m_i \rangle}{(E_f - E_s)^2}, \quad (4.5)$$

$$\langle \sigma_L | V | n\Gamma_i m_i \rangle \equiv \langle n f^0; \sigma_L | V | n f^1 \Gamma_i m_i; \sigma_L \rangle, \quad (4.6)$$

and for the processes 4*f*<sup>1</sup>*L* → 4*f*<sup>2</sup> as

$$\langle n\Gamma_j m_j | \sigma_\alpha | n\Gamma_i m_i \rangle \equiv - \sum_{\sigma_L \sigma'_L} \frac{\langle \sigma_L | \sigma_\alpha | \sigma'_L \rangle \langle \sigma_L | V | n\Gamma_j m_j \rangle^* \langle \sigma'_L | V | n\Gamma_i m_i \rangle}{(E_f + U - E_s)^2}, \quad (4.7)$$

$$\langle \sigma_L | V | n\Gamma_i m_i \rangle \equiv \sum_{\Gamma' m'} \langle n f^2 \Gamma' m' | V | n f^1 \Gamma_i m_i; \sigma_L \rangle, \quad (4.8)$$

where *U* is the intraatomic Coulomb repulsion between 4*f* electrons, and  $\sigma_L$  is the spin quantum number of the ligand *s* orbital. We take into account of only the Hund rule ground state in the 4*f*<sup>2</sup> configuration and neglect the CF energy splitting in the denominators of eqs. (4.5) and (4.7). From eqs. (3.5) and (4.4), it is deduced that the ligand spin polarization is not proportional to the single-ion susceptibility, while the spin polarization is linear to the susceptibility and isotropic in the high temperature limit. These behaviors qualitatively agree with the temperature-dependent hyperfine coupling in CeCu<sub>2</sub>Si<sub>2</sub> and YbCu<sub>2</sub>Si<sub>2</sub>. At lower temperatures than the splitting energy between the ground and the first-excited states, the temperature dependence of both spin polarization and

susceptibility is given by a Curie term. Therefore the *K* -  $\chi$  plot is again linear in the low-temperature limit. In CeCu<sub>2</sub>Si<sub>2</sub> the temperature range between 10 and 50K possibly corresponds to this low-temperature limit.

We now show that the spin polarization can be anisotropic and that it can reverse its sign in the low-temperature limit depending on the ground state wave functions. Considering the  $\Gamma_7^{(1)}$  ground state in the CF of eq. (3.1), the temperature-dependent terms in the low-temperature limit are

$$\begin{aligned} \langle \sigma_z \rangle & \sim -\frac{g_J \mu_B \beta H}{Z} (4\eta^2 - \frac{3}{2}) \sum_n [\langle n, +\frac{5}{2} | \sigma_z | n, +\frac{5}{2} \rangle - \langle n, -\frac{5}{2} | \sigma_z | n, -\frac{5}{2} \rangle], \\ \langle \sigma_x \rangle & \sim -\frac{g_J \mu_B \beta H}{Z} \sqrt{5} \eta \sqrt{1 - \eta^2} \sum_n [\langle n, -\frac{5}{2} | \sigma_x | n, +\frac{5}{2} \rangle - \langle n, +\frac{5}{2} | \sigma_x | n, -\frac{5}{2} \rangle]. \end{aligned} \quad (4.9)$$

We calculate the ligand spin polarization by four nearest-neighbor Ce ion for the atomic configurations of the Cu and Si sites below. We here define the anisotropy factors  $F_\alpha(\eta)$  as

$$\begin{aligned} \langle \sigma_\alpha \rangle & \equiv -\frac{g_J \mu_B \beta H}{Z} \frac{(sf\sigma)^2}{(E_f + U - E_s)^2} F_\alpha(\eta) \quad (4f^1 L \rightarrow 4f^2), \\ \langle \sigma_\alpha \rangle & \equiv -\frac{g_J \mu_B \beta H}{Z} \frac{(sf\sigma)^2}{(E_f - E_s)^2} F_\alpha(\eta) \quad (4f^1 L \rightarrow 4f^0). \end{aligned} \quad (4.10)$$

For the Cu sites, we obtain for the processes 4*f*<sup>1</sup>*L* → 4*f*<sup>2</sup>

$$\begin{aligned} F_z(\eta) & = (4\eta^2 - \frac{3}{2})(-0.72 + 3.23\eta^2 - 1.39\eta\sqrt{1 - \eta^2}), \\ F_x(\eta) & = \sqrt{5}\eta\sqrt{1 - \eta^2}(-1.07 - 0.92\eta^2 + 3.81\eta\sqrt{1 - \eta^2}), \end{aligned} \quad (4.11)$$

and for 4*f*<sup>1</sup> → 4*f*<sup>0</sup>*L*

$$\begin{aligned} F_z(\eta) & = (4\eta^2 - \frac{3}{2})(-0.52 + 0.42\eta^2 - 0.47\eta\sqrt{1 - \eta^2}), \\ F_x(\eta) & = \sqrt{5}\eta\sqrt{1 - \eta^2}(0.19 - 0.29\eta^2 - 0.47\eta\sqrt{1 - \eta^2}), \end{aligned} \quad (4.12)$$

where (*sfσ*) is the Slater-Koster integral and we used the Slater-Koster tables for *f* electrons given in ref. [69]. For the Si sites, we obtain for the processes 4*f*<sup>1</sup>*L* → 4*f*<sup>2</sup>

$$\begin{aligned} F_z(\eta) & = (4\eta^2 - \frac{3}{2})(-0.23 + 0.26\eta^2 - 0.19\eta\sqrt{1 - \eta^2}), \\ F_x(\eta) & = \sqrt{5}\eta\sqrt{1 - \eta^2}(-0.64 - 0.09\eta^2 + 1.53\eta\sqrt{1 - \eta^2}), \end{aligned} \quad (4.13)$$

and for 4*f*<sup>1</sup> → 4*f*<sup>0</sup>*L*

$$\begin{aligned} F_z(\eta) & = (4\eta^2 - \frac{3}{2})(0.56 - 1.12\eta^2 - 0.32\eta\sqrt{1 - \eta^2}), \\ F_x(\eta) & = \sqrt{5}\eta\sqrt{1 - \eta^2}(0.57 - 0.46\eta^2 - 0.51\eta\sqrt{1 - \eta^2}). \end{aligned} \quad (4.14)$$

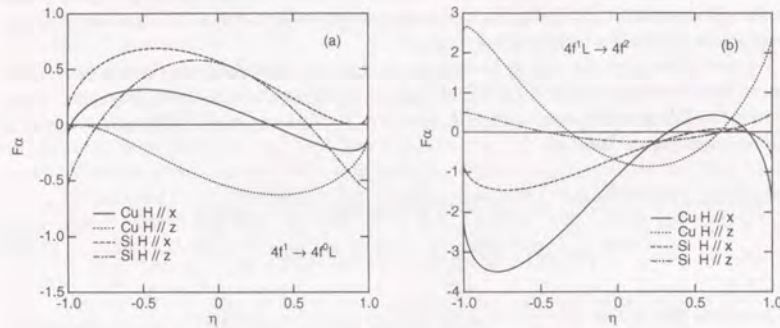


Figure 4.1. Anisotropy factor  $F_\alpha(\eta)$  for the Cu and Si sites, (a) for the process  $4f^1 \rightarrow 4f^0 L$ , (b) for the process  $4f^1 L \rightarrow 4f^2$ .

In the low-temperature limit, the temperature-dependent terms in the susceptibilities are

$$\chi_z = \frac{g_J^2 \mu_B^2}{Z} \beta \cdot 2 \left( \frac{3}{2} - 4\eta^2 \right)^2, \quad (4.15)$$

$$\chi_x = \frac{g_J^2 \mu_B^2}{Z} \beta \cdot 10\eta^2 (1 - \eta^2). \quad (4.16)$$

The transferred hyperfine coupling is given by  $A_\alpha = -gA_s(\sigma_\alpha)/\chi H$ , where  $A_s$  is the hyperfine coupling of the ligand  $s$  orbital and the ligand nucleus. In Fig. 4.1, we present the  $\eta$  dependence of the anisotropy factors. Since the susceptibility is positive independently of  $\eta$ , we can evaluate the sign of the hyperfine coupling with these values. The results clearly show that the hyperfine coupling strongly depends on  $\eta$  and that it can change in sign, giving a qualitative explanation of the negative hyperfine coupling observed in  $\text{CeCu}_2\text{Si}_2$ . This also explains the site dependence of the observed hyperfine coupling.

The hyperfine couplings at the low temperatures in  $\text{CeCu}_2\text{Si}_2$  are the same order of magnitude as in  $\text{GdCu}_2\text{Si}_2$ . For the simple  $s$ - $f$  exchange model eq. (1.7), the hyperfine coupling is proportional to the factor  $(g_J - 1)/g_J$ ;  $-\frac{1}{6}$  for  $\text{CeCu}_2\text{Si}_2$  and  $-\frac{1}{2}$  for  $\text{GdCu}_2\text{Si}_2$ . The observed strong hyperfine couplings in  $\text{CeCu}_2\text{Si}_2$  also suggest the direct hybridization of the  $f$  electrons.

#### 4.4 $f$ -Ligand Hybridization in $\text{PrCu}_2\text{Si}_2$

The hyperfine couplings in  $\text{PrCu}_2\text{Si}_2$  are different in sign and magnitude from those in  $\text{GdCu}_2\text{Si}_2$ . When the hyperfine coupling between the conduction electrons and the Cu or Si nuclei is not different between those in  $\text{PrCu}_2\text{Si}_2$  and  $\text{GdCu}_2\text{Si}_2$ , the change in

sign can be explained with the  $s$ - $f$  exchange model eq. (1.7). The factor  $g_J - 1$  gives the opposite signs for  $\text{Gd}^{3+}$  ( $g_J = 2$ ) and  $\text{Pr}^{3+}$  ( $g_J = 0.8$ ), but the magnitude estimation is not satisfactory especially for the Si sites. The ratio  $^{29}A_\alpha/^{63}A_\alpha$  ( $\alpha$  is  $\parallel$  or  $\perp$ ) is remarkably different between  $\text{PrCu}_2\text{Si}_2$  and  $\text{GdCu}_2\text{Si}_2$ . This cannot be explained by the change in the  $s$ - $f$  exchange energy only. The enhanced hyperfine coupling at the Si sites in  $\text{PrCu}_2\text{Si}_2$  suggests the strong hybridization of the  $f$ -electrons with the Si valence electrons. It was recently argued that the Si contribution to the CF potential substantially increases in  $\text{PrCu}_2\text{Si}_2$  in comparison with  $\text{NdCu}_2\text{Si}_2$  [49]. This observation likely supports the enhanced hybridization of the  $f$  electrons. The change in the anisotropy of the hyperfine couplings in comparison between  $\text{PrCu}_2\text{Si}_2$  and  $\text{GdCu}_2\text{Si}_2$  also suggests the hybridization effect.

This hybridization is possibly responsible for the strong two-ion coupling in  $\text{PrCu}_2\text{Si}_2$ , which causes the unusually high Néel temperature. We here examine the anisotropy of  $\Theta$  in  $\text{PrCu}_2\text{Si}_2$ . The CF effect can cause the anisotropy of  $\Theta$ . For the  $D_{4h}$  symmetry at the Pr sites, the CF Hamiltonian is written with operator equivalents of  $\mathbf{J}$  as

$$H_{cf} = B_2^0 O_2^0 + B_4^0 O_4^0 + B_4^4 O_4^4 + B_6^0 O_6^0 + B_6^4 O_6^4. \quad (4.17)$$

This gives anisotropic  $\Theta$  in the high-temperature limit as

$$\Theta_{\parallel} = \frac{J(J+1)}{3k_B} J_{ff} - \frac{12}{5} \left( J - \frac{1}{2} \right) \left( J + \frac{3}{2} \right) B_2^0, \quad (4.18)$$

and

$$\Theta_{\perp} = \frac{J(J+1)}{3k_B} J_{ff} + \frac{6}{5} \left( J - \frac{1}{2} \right) \left( J + \frac{3}{2} \right) B_2^0, \quad (4.19)$$

where  $J_{ff}$  is the two-ion exchange energy and is assumed to be isotropic here. The direct dipolar contribution to  $J_{ff}$  is estimated to be below 0.1K from eq. (3.10). If the CF effect dominates the anisotropy of  $\Theta$ , we obtain  $B_2^0 \sim -0.84\text{K}$  and  $J_{ff} \sim -0.97\text{K}$ . The deduced value of  $B_2^0$  agrees well with the CF parameters measured by the neutron-scattering measurements  $B_2^0 \sim -0.73\text{K}$  [49]. Thus the anisotropy of  $\Theta$  is mainly ascribed to the one-ion anisotropy. As mentioned in Sect. 1.2.1, the mixing interaction can cause the anisotropy of two-ion coupling. However, the two-ion coupling, which cause the remarkably high  $T_N$ , is almost isotropic in  $\text{PrCu}_2\text{Si}_2$ .

In the previous subsection, we argued that the direct  $f$ -ligand hybridization may cause the temperature-dependent hyperfine coupling in co-operation with the large CF splitting. The temperature dependence is not observed in  $\text{PrCu}_2\text{Si}_2$  in spite of the enhanced  $f$ -ligand hybridization. This is considered to be due to the small CF splitting.

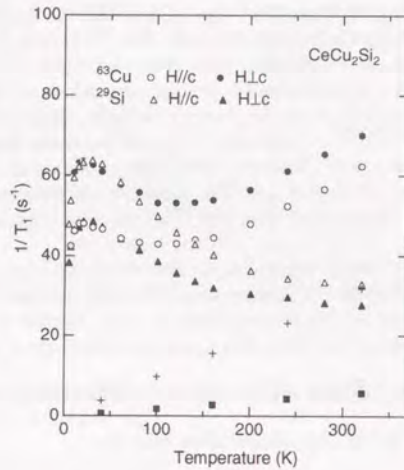


Figure 5.1. Temperature dependence of  $1/T_1$  at Cu and Si sites in  $\text{CeCu}_2\text{Si}_2$ , and at Cu (+) and Si (■) sites in  $\text{YCu}_2\text{Si}_2$  for  $H \perp c$ .

## 5 Nuclear Relaxation Measurements

In the previous section, we have discussed the mechanism of the temperature-dependent hyperfine coupling in  $\text{CeCu}_2\text{Si}_2$  and  $\text{YbCu}_2\text{Si}_2$ . In this section, we will describe the  $T_1$  measurements on these compounds. We investigate the effect of the temperature-dependent hyperfine coupling on the nuclear relaxation rates by measuring the anisotropy and the site dependence of  $T_1$  in these compounds.

### 5.1 $\text{CeCu}_2\text{Si}_2$

The temperature dependence of  $1/T_1$  at the Cu and Si sites is measured for  $H \parallel c$  and  $H \perp c$ ; the results are shown in Fig. 5.1. The previous result of  $^{29}(1/T_1)$  measured with a powder sample [35] qualitatively agrees with the present data. In general, when the hyperfine coupling is temperature-independent and the spatial correlation is negligible, it is expected that the nuclear relaxation rates at the inequivalent atomic sites are proportional to each other. In  $\text{CeCu}_2\text{Si}_2$ , however, from the observed temperature-dependent hyperfine coupling, it is expected that the temperature dependence of  $1/T_1$  at the Cu and Si sites differs. Actually the measured relaxation rates at both the sites behave differently at high temperatures. To examine this site dependence,  $^{29}(1/T_1T)$  is

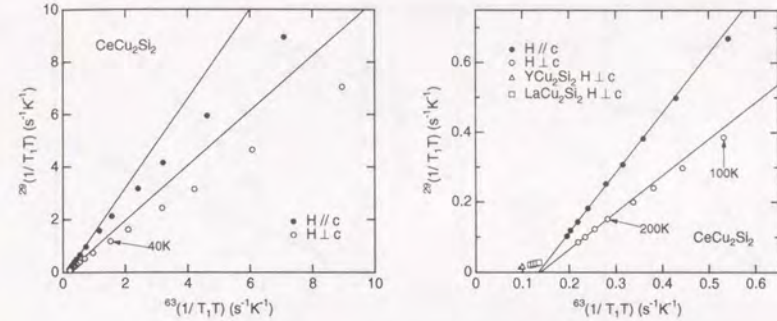


Figure 5.2.  $^{29}(1/T_1T)$  is plotted against  $^{63}(1/T_1T)$  for  $\text{CeCu}_2\text{Si}_2$ : (a) the whole data, (b) high temperature data. Solid lines are linear fitting results above 200K.

plotted against  $^{63}(1/T_1T)$  in Fig. 5.2 (a) and (b). It is found that the plots are linear at high temperatures. Furthermore, the deviation from the linearity at low temperatures is weak.

The extrapolated line of the linear fitting of  $^{29}(1/T_1T)$  against  $^{63}(1/T_1T)$  for  $H \perp c$  is close to the data for  $\text{YCu}_2\text{Si}_2$  and  $\text{LaCu}_2\text{Si}_2$ , while it does not approach the origin. This suggests that the nuclear relaxation rates in  $\text{CeCu}_2\text{Si}_2$  are described as the sum of the contributions of the  $4f$  electrons and the conduction electrons,

$$\frac{1}{T_1T} = \left(\frac{1}{T_1T}\right)_f + \left(\frac{1}{T_1T}\right)_c. \quad (5.1)$$

The  $f$  electron contribution is responsible for the temperature dependence of  $1/T_1T$ , while the conduction-electron contribution is almost temperature-independent and its value is near that in  $\text{YCu}_2\text{Si}_2$  and  $\text{LaCu}_2\text{Si}_2$ . The experimental result shows that the  $f$  contributions at the Cu and the Si sites are almost proportional to each other and that the strong site dependence of  $1/T_1$  at high temperatures is ascribed to the large difference of  $(1/T_1T)_c$  at the Si and Cu sites.

It was observed that the anisotropy of the temperature dependence of  $1/T_1$  is weak. To examine the anisotropy, we define the relaxation rates

$$\left(\frac{1}{T_1T}\right)_{\parallel} = 2\left(\frac{1}{T_1T}\right)_{H \perp c} - \left(\frac{1}{T_1T}\right)_{H \parallel c}, \quad (5.2)$$

$$\left(\frac{1}{T_1T}\right)_{\perp} = \left(\frac{1}{T_1T}\right)_{H \parallel c}. \quad (5.3)$$

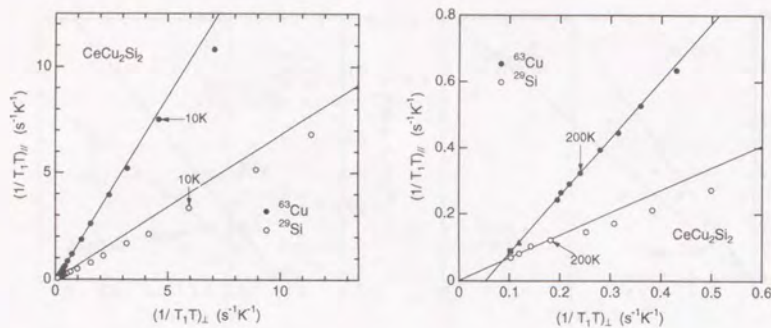


Figure 5.3. Anisotropy of  $1/T_1T$  in  $\text{CeCu}_2\text{Si}_2$ : (a) the whole data, (b) high temperature data. Solid triangle: for  $^{63}\text{Cu}$  in  $\text{LaCu}_2\text{Si}_2$  ( $\blacktriangle$ ), in  $\text{YCu}_2\text{Si}_2$  ( $\blacksquare$ ). Solid lines are linear fitting results above 200K.

These relaxation rates can be written using the anisotropic hyperfine field as

$$\left(\frac{1}{T_1T}\right)_{\parallel} = \frac{\gamma_N^2}{2T} \int_{-\infty}^{\infty} dt e^{i\omega_N t} \langle \{H_{\text{hf}}^{\parallel}(t) H_{\text{hf}}^{\parallel}\} \rangle, \quad (5.4)$$

$$\left(\frac{1}{T_1T}\right)_{\perp} = \frac{\gamma_N^2}{2T} \int_{-\infty}^{\infty} dt e^{i\omega_N t} \langle \{H_{\text{hf}}^{\perp}(t) H_{\text{hf}}^{\perp}\} \rangle, \quad (5.5)$$

where  $H_{\text{hf}}^{\perp}$  and  $H_{\text{hf}}^{\parallel}$  are the component in the basal plane and along the  $c$ -axis of the fluctuating hyperfine field, respectively.  $(1/T_1T)_{\parallel}$  is plotted against  $(1/T_1T)_{\perp}$  in Figs. 5.3 (a) and 5.3 (b). These plots are approximately linear. This also contrasts with the strong temperature dependence of the anisotropy of the hyperfine coupling. The extrapolation of the fitting for the  $^{63}\text{Cu}$  sites at high temperatures reaches the values for  $\text{YCu}_2\text{Si}_2$  and  $\text{LaCu}_2\text{Si}_2$ . This result justifies the separation of the  $f$ -electron and the conduction-electron contributions.

The observed weak changes in the anisotropy and the site dependence seem to conflict with the observed temperature-dependent hyperfine coupling. This problem will be discussed in a later section.

## 5.2 $\text{YbCu}_2\text{Si}_2$

The temperature dependence of  $1/T_1$  at the Cu and Si sites for  $H \parallel c$  and  $H \perp c$  is shown in Fig. 5.4. To discuss the site dependence of  $1/T_1$ ,  $^{29}(1/T_1T)$  is plotted against  $^{63}(1/T_1T)$  in Fig. 5.5. These plots are linear at high temperatures, but a weak deviation appears below about 100K. The extrapolated line of the linear fitting of  $^{29}(1/T_1T)$  against

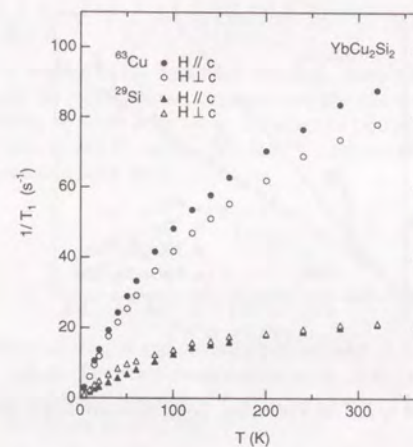


Figure 5.4. Temperature dependence of  $1/T_1$  at Cu and Si sites in  $\text{YbCu}_2\text{Si}_2$ .

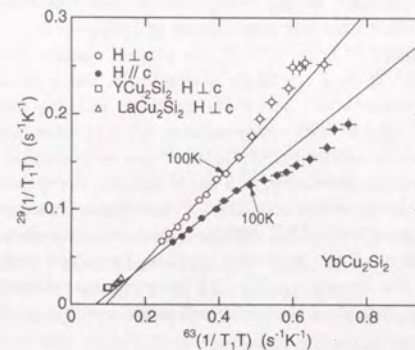


Figure 5.5.  $^{29}(1/T_1T)$  is plotted against  $^{63}(1/T_1T)$  for  $\text{YbCu}_2\text{Si}_2$ . Solid lines are linear fitting results above 120K.

$^{63}(1/T_1T)$  above 120K for  $H \perp c$  is near the results for  $\text{YCu}_2\text{Si}_2$  and  $\text{LaCu}_2\text{Si}_2$ , and it does

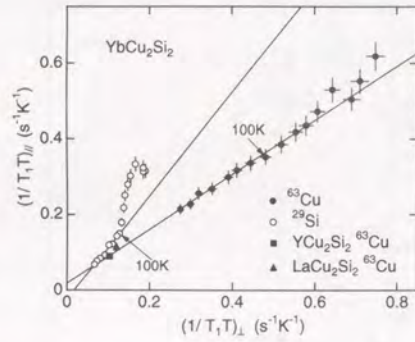


Figure 5.6. Anisotropy of  $1/T_1T$  in  $\text{YbCu}_2\text{Si}_2$ . Solid lines are linear fitting results above 120K.

not reach the origin. This suggests that the nuclear relaxation rates are described as the sum of the contributions of the  $4f$  electrons and the conduction electrons in  $\text{YbCu}_2\text{Si}_2$ , as well as in  $\text{CeCu}_2\text{Si}_2$ . Therefore, at high temperatures, the conduction-electron contribution is mainly responsible for the site dependence of  $1/T_1$ .

To examine the anisotropy of  $1/T_1$ ,  $(1/T_1T)_\parallel$  is plotted against  $(1/T_1T)_\perp$  in Fig. 5.6. These plots for the Cu and Si sites are linear above 100K, but a clear deviation is seen at the Si sites at low temperatures. The  $^{63}\text{Cu}$  data for  $\text{YCu}_2\text{Si}_2$  and  $\text{LaCu}_2\text{Si}_2$  lie on the extrapolation of the fitting at high temperatures. This justifies the separation of the  $f$ -electron and the conduction electron contributions also in  $\text{YbCu}_2\text{Si}_2$ .

Development of the spatial correlation can cause the site dependence of  $1/T_1$  via the different  $q$ -dependence of the hyperfine couplings. When  $\chi(q, \omega)$  is enhanced in a region of  $q$  space as decreasing temperature,  $1/T_1T$  will increase more strongly at the nuclear sites where the same  $q$  component of the hyperfine coupling has larger weight. However, the observed deviations from the linearity in Fig. 5.5 have opposite directions depending on the external field direction, indicating that this mechanism seems improbable in  $\text{YbCu}_2\text{Si}_2$ .

### 5.3 Discussion

At first, we discuss the observed anisotropy and site dependence in  $\text{CeCu}_2\text{Si}_2$  and  $\text{YbCu}_2\text{Si}_2$  with the conventional form eq. (1.11) on the assumption that  $\chi(q, \omega)$  is  $q$ -independent.

Neglecting the  $q$  dependence, two distinct ratios of  $1/T_1T$  are written as

$${}^{29}\left(\frac{1}{T_1T}\right)_\alpha^f / {}^{63}\left(\frac{1}{T_1T}\right)_\alpha^f = \left(\frac{{}^{29}\gamma_N}{{}^{63}\gamma_N}\right)^2 \left| \frac{\langle {}^{29}A_\alpha \rangle_q}{{}^{63}A_\alpha} \right|^2 \quad (\alpha = \perp, \parallel), \quad (5.6)$$

and

$${}^n\left(\frac{1}{T_1T}\right)_\parallel^f / {}^n\left(\frac{1}{T_1T}\right)_\perp^f = \left| \frac{\langle {}^nA_\parallel \rangle_q}{{}^nA_\perp} \right|^2 \frac{\chi_\parallel''}{\chi_\perp''} \quad (n = 29, 63), \quad (5.7)$$

where  $\langle A \rangle_q$  is the  $q$  average of the hyperfine coupling. Assuming that the  $q$  dependence of  $A_\alpha$  is insignificant, we replace these averages with the  $q = 0$  components.

The former relation eq. (5.6) is obviously incorrect in  $\text{CeCu}_2\text{Si}_2$ , because the hyperfine coupling is almost zero at the Cu sites, while the  $^{63}\text{Cu}$  relaxation rates are comparable to the  $^{29}\text{Si}$  rates; we obtain above 200K

$$\begin{aligned} {}^{29}\left(\frac{1}{T_1T}\right)_\parallel^f / {}^{63}\left(\frac{1}{T_1T}\right)_\parallel^f &\sim 0.67, \\ {}^{29}\left(\frac{1}{T_1T}\right)_\perp^f / {}^{63}\left(\frac{1}{T_1T}\right)_\perp^f &\sim 1.7. \end{aligned} \quad (5.8)$$

Even if the hyperfine coupling is significantly  $q$ -dependent, it is impossible that only its  $q \sim 0$  components vanish. Thus this disagreement in eq. (5.6) cannot be explained by the  $q$  dependence of the hyperfine coupling.

For  $\text{YbCu}_2\text{Si}_2$ , we obtain above 120K

$$\begin{aligned} {}^{29}\left(\frac{1}{T_1T}\right)_\parallel^f / {}^{63}\left(\frac{1}{T_1T}\right)_\parallel^f &\sim 0.60, \\ {}^{29}\left(\frac{1}{T_1T}\right)_\perp^f / {}^{63}\left(\frac{1}{T_1T}\right)_\perp^f &\sim 0.32, \end{aligned} \quad (5.9)$$

and using the hyperfine couplings in Table 3.2,

$$\begin{aligned} \left(\frac{{}^{29}\gamma_N}{{}^{63}\gamma_N}\right)^2 \left| \frac{{}^{29}A_\parallel}{{}^{63}A_\parallel} \right|^2 &\sim 0.046, \\ \left(\frac{{}^{29}\gamma_N}{{}^{63}\gamma_N}\right)^2 \left| \frac{{}^{29}A_\perp}{{}^{63}A_\perp} \right|^2 &\sim 0.27. \end{aligned} \quad (5.10)$$

These ratios disagree with each other.

From the latter relation, we can estimate the ratio  $\chi_\parallel''/\chi_\perp''$ . We obtain  $\chi_\parallel''/\chi_\perp'' \sim 3.3$  from the  $^{63}\text{Cu}$  results and 1.1 from the  $^{29}\text{Si}$  results. These disagreements provide an evidence that we cannot write  $1/T_1$  as eq. (1.11) also in  $\text{YbCu}_2\text{Si}_2$ .

We have found that eq. (1.11) fails in these compounds even at the high temperatures, where the  $f$  contributions to  $1/T_1T$  at the Cu and Si sites are proportional. Next, let us consider the temperature dependence of the hyperfine coupling on the basis of the  $f$ -ligand hybridization. When the CF splitting of  $4f$  levels exists, the single site dynamical susceptibility is written as the sum of Curie and Van Vleck terms [44, 70],

$$\begin{aligned} \chi_\alpha''(\omega) &= \sum_{\Gamma_i} \chi_\alpha^{C''}(\omega; \Gamma_i) + \frac{1}{2} \sum_{\Gamma_i} \sum_{\Gamma_j} \chi_\alpha^{V''}(\omega; \Gamma_i, \Gamma_j) \quad (\alpha = x, y, z), \quad (5.11) \\ \chi_\alpha^{C''}(\omega; \Gamma_i) &= \frac{\pi g_J^2 \mu_B^2}{Z} (1 - e^{-\beta \hbar \omega}) \sum_{m_i} \sum_{m_i'} |\langle \Gamma_i m_i | J_\alpha | \Gamma_i m_i' \rangle|^2 \end{aligned}$$

$$\times \int_{-\infty}^{\infty} d\omega' e^{-\beta\hbar\omega'} \rho_{\Gamma_i}(\omega') \rho_{\Gamma_i}(\omega' + \omega), \quad (5.12)$$

$$\chi_{\alpha}^{V''}(\omega; \Gamma_i, \Gamma_j) = \frac{\pi g_J^2 \mu_B^2}{Z} (1 - e^{-\beta\hbar\omega}) \sum_{m_i, m_j} |\langle \Gamma_i m_i | J_{\alpha} | \Gamma_j m_j \rangle|^2 \times \int_{-\infty}^{\infty} d\omega' e^{-\beta\hbar\omega'} \rho_{\Gamma_i}(\omega') \rho_{\Gamma_j}(\omega' + \omega), \quad (5.13)$$

where  $\rho_{\Gamma_i}(\omega)$  is the spectral density of the  $\Gamma_i$  state. When the transferred hyperfine coupling is due to the  $f$ -ligand hybridization, the Curie and the Van Vleck terms in the susceptibility have distinct hyperfine couplings, as seen in eq. (4.4). Then each term in eq. (5.11) contributes to the nuclear relaxation rate with a different hyperfine coupling. The  $f$  contribution to the nuclear relaxation rate is written as

$$\left(\frac{1}{T_1 T}\right)_{\alpha}^f = \frac{N \gamma_N^2 k_B}{2 \mu_B^2} \left[ \sum_{\Gamma_i} |A_{\alpha}^C(\Gamma_i)|^2 \frac{\chi_{\alpha}^{C''}(\omega_N; \Gamma_i)}{\omega_N} + \frac{1}{2} \sum_{\Gamma_i, \Gamma_j} |A_{\alpha}^V(\Gamma_i, \Gamma_j)|^2 \frac{\chi_{\alpha}^{V''}(\omega_N; \Gamma_i, \Gamma_j)}{\omega_N} \right]. \quad (5.14)$$

Since usually  $\omega_N$  is very low, the Van Vleck terms is negligible. When the occupation of the CF states significantly changes as temperature, it is expected that the anisotropy and the site dependence of  $1/T_1$  change accordingly. This is a similar origin to that proposed for the temperature-dependent hyperfine coupling in Sec. 4.3. With this mechanism, we can qualitatively explain the changes in the anisotropy and the site dependence of the nuclear relaxation rates in  $\text{YbCu}_2\text{Si}_2$ . As seen in Figs. 5.5 and 5.6, these changes appear in the same temperature region around 100K as the hyperfine coupling. This supports our explanation. It is clearly seen from eq. (5.14) that the sum of the hyperfine couplings, which is to be experimentally observed at the high temperature limit, cannot be used to estimate the anisotropy or the site dependence of  $1/T_1$ . Therefore the discrepancy between the relaxation rate ratios and the hyperfine coupling at the high temperatures is reasonable.

In  $\text{CeCu}_2\text{Si}_2$ , the  $^{63}\text{Cu}$  relaxation rates are considerably large at high temperatures in spite of almost zero hyperfine couplings. This can be qualitatively explained as follows: the Curie and the Van Vleck terms in the hyperfine coupling cancel each other at the Cu sites, but the Curie terms in the relaxation rates eq. (5.14) are always added up and give a considerable relaxation rates.

Then, why are the changes in the anisotropy and the site dependence rather weak in  $\text{CeCu}_2\text{Si}_2$ ? One possible explanation is that the excited Curie terms in eq. (5.14) give only small contributions for some reason. Then the  $4f$  contribution in  $1/T_1 T$  is written as

$$\left(\frac{1}{T_1 T}\right)_{\alpha}^f = \frac{N \gamma_N^2 k_B}{2 \mu_B^2} |A_{\alpha}^g|^2 \frac{\chi_{\alpha}^{g''}(\omega_N)}{\omega_N} \quad (\alpha = \perp, \parallel), \quad (5.15)$$

where  $A_{\alpha}^g$  and  $\chi_{\alpha}^{g''}$  are the ground doublet contributions. If  $\chi(\omega)^g$  is described with a Lorentzian form

$$\chi^g(\omega) = \frac{\chi^g}{1 - i\omega/\Gamma}, \quad (5.16)$$

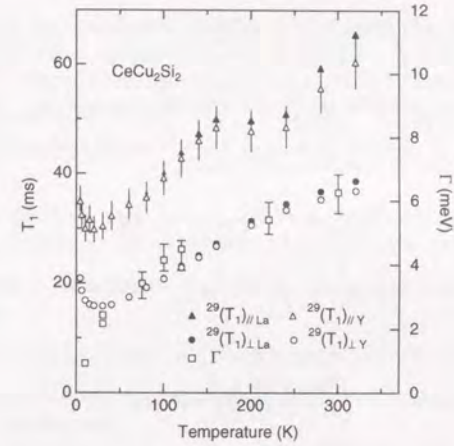


Figure 5.7. Temperature dependence of  $f$  contributions to  $T_1$ . Quasielastic line half width  $\Gamma$  [32] is also shown.

we obtain

$$\left(\frac{1}{T_1}\right)^f = \frac{N \gamma_N^2 k_B T}{2 \mu_B^2} |A^g|^2 \frac{\chi^g}{\Gamma}. \quad (5.17)$$

We here neglect the anisotropy of  $1/T_1$ ,  $\chi^g$  and the hyperfine coupling. Assuming that a Curie law for the ground doublet  $\chi^g \propto T^{-1}$ , we obtain

$$\left(\frac{1}{T_1}\right)^f \propto \frac{1}{\Gamma}. \quad (5.18)$$

We can estimate  $(1/T_1)^f$  by subtracting the relaxation rates in  $\text{YCu}_2\text{Si}_2$  or  $\text{LaCu}_2\text{Si}_2$  from the experimental results. The results for the Si sites and  $\Gamma$  deduced from the neutron scattering measurement [32] are plotted in Fig. 5.7. We here neglected the anisotropy of  $T_1$  in  $\text{YCu}_2\text{Si}_2$  and  $\text{LaCu}_2\text{Si}_2$ . It is found that  $T_1$  is roughly proportional to  $\Gamma$  above 70K. The disagreement at low temperatures is partly due to the assumed Curie susceptibility. Aarts *et al.* obtained the  $T$ -linear effective relaxation time of  $4f$  moments using the observed  $^{29}\text{K}$  instead of the Curie-like  $\chi^g$  [35], and compared it to the temperature dependence of  $\Gamma$ . Since the Knight shift and the magnetic susceptibility include the Van Vleck terms, they are obviously inadequate for the estimate of  $\Gamma$ .

Well below the CF splitting temperature,  $1/T_1$  should be dominated by the Curie term of the ground doublet. The hyperfine couplings  $A_{\alpha}^g$  can be estimated from the  $K-\chi$  plot

at low temperatures. Then the similar ratios of  $1/T_1T$  as eqs. (5.6) and (5.7) are written as

$${}^{29}\left(\frac{1}{T_1T}\right)_\alpha^f / {}^{63}\left(\frac{1}{T_1T}\right)_\alpha^f = \left(\frac{{}^{29}\gamma_N}{{}^{63}\gamma_N}\right)^2 \left|\frac{{}^{29}A_\alpha^g}{{}^{63}A_\alpha^g}\right|^2 \quad (\alpha = \perp, \parallel), \quad (5.19)$$

$${}^n\left(\frac{1}{T_1T}\right)_\parallel^f / {}^n\left(\frac{1}{T_1T}\right)_\perp^f = \left|\frac{{}^nA_\parallel^g}{{}^nA_\perp^g}\right|^2 \frac{\chi_\parallel^{g''}}{\chi_\perp^{g''}} \quad (n = 29, 63). \quad (5.20)$$

For the former relation, we experimentally obtain

$$\begin{aligned} {}^{29}\left(\frac{1}{T_1T}\right)_\parallel^f / {}^{63}\left(\frac{1}{T_1T}\right)_\parallel^f &\sim 0.45, \\ {}^{29}\left(\frac{1}{T_1T}\right)_\perp^f / {}^{63}\left(\frac{1}{T_1T}\right)_\perp^f &\sim 1.26, \end{aligned} \quad (5.21)$$

and

$$\begin{aligned} \left(\frac{{}^{29}\gamma_N}{{}^{63}\gamma_N}\right)^2 \left|\frac{{}^{29}A_\parallel^g}{{}^{63}A_\parallel^g}\right|^2 &\sim 0.11, \\ \left(\frac{{}^{29}\gamma_N}{{}^{63}\gamma_N}\right)^2 \left|\frac{{}^{29}A_\perp^g}{{}^{63}A_\perp^g}\right|^2 &\sim 10.2. \end{aligned} \quad (5.22)$$

The discrepancy is very large. From the latter relation with the hyperfine coupling in Table 3.1, we obtain  $\chi_\parallel^{g''}/\chi_\perp^{g''} \sim 0.21$  from the  ${}^{63}\text{Cu}$  results, and 6.5 from the  ${}^{29}\text{Si}$  results in  $\text{CeCu}_2\text{Si}_2$ . We have large discrepancy again.

These failures of the estimations indicate that we cannot estimate the anisotropy and the site dependence of nuclear relaxation rates from the hyperfine coupling experimentally obtained at low temperatures. This may be because the hyperfine couplings in eq. (5.14) differ intrinsically from those defined by eqs. (3.5) and (4.4).

We have neglected the spatial correlation of the Ce moments in the analysis so far, it may be responsible for the above discrepancy at low temperatures. The qualitative analysis including the spatial correlation is a remaining problem.

## 6 Conclusion

We have studied the temperature-dependent transferred hyperfine coupling in the  $\text{RCu}_2\text{Si}_2$  series of rare-earth intermetallic compounds.

In  $\text{CeCu}_2\text{Si}_2$ , we have observed the temperature-dependent hyperfine coupling at both the Cu and Si sites. The following properties have been emerged:

- The temperature dependence of the Knight shifts at both the sites is significantly different.
- The slope of the  $K-\chi$  plots changes with temperature, but is approximately constant in the temperature ranges between about 10 and 50K and above about 200K.
- The anisotropy of the hyperfine couplings at both the sites is remarkable at the low temperatures.
- The hyperfine coupling along the  $c$ -axis is negative at both the sites.
- The enhancement of the hyperfine coupling below  $T_K$ , which was previously reported, was not observed.

In  $\text{YbCu}_2\text{Si}_2$ , we have also observed the temperature-dependent hyperfine coupling at the Si sites, as well as at the Cu sites. We have obtained the following results:

- The temperature dependence of the Knight shifts at both the sites are significantly different.
- The anisotropy of the hyperfine couplings at the Si sites is remarkable at the low temperatures.

We have pointed out an empirical rule on the transferred hyperfine coupling in rare-earth compounds, that is, the hyperfine coupling is positive for rare-earth ions with  $J = L - S$  and negative for  $J = L + S$  regardless of the ligand atoms and the crystal structures. From this rule it follows that the transferred hyperfine coupling is dominated by the  $s$  spin polarization at the ligand sites. Furthermore, this spin polarization is due to the polarization of the  $5s$  and  $5p$  outer shells. The negative hyperfine coupling in  $\text{CeCu}_2\text{Si}_2$  is the only exception to this empirical rule, suggesting the direct  $f$ -ligand  $s$  hybridization.

We have proposed a mechanism of the temperature-dependent hyperfine coupling based on this direct hybridization, where each of the Curie and the Van Vleck terms in the one-ion susceptibility contributes to the Knight shift with different hyperfine couplings. The resulting hyperfine coupling varies with temperature according to the occupation of the CF levels. At low temperatures where only the ground CF levels are predominantly occupied, the hyperfine coupling is temperature-independent, and has site dependence and an anisotropy, which depend on the ground state orbitals and the ligand atomic positions. Furthermore, it has been shown from the present model that the hyperfine coupling can change in its sign. At high temperatures where all the CF levels are equally occupied, the hyperfine coupling is intrinsically isotropic. These properties qualitatively agree with the experimental results.

In  $\text{PrCu}_2\text{Si}_2$  and  $\text{GdCu}_2\text{Si}_2$ , we have observed the linear  $K - \chi$  plots, but the anisotropy and the site dependence are different between these compounds. It has been found that the hyperfine coupling at the Si sites is relatively enhanced in  $\text{PrCu}_2\text{Si}_2$ . This indicates the preferential hybridization of the  $f$ -electrons with the Si valence electrons in  $\text{PrCu}_2\text{Si}_2$ . This hybridization is probably responsible for the remarkably high Néel temperature. The temperature-dependent hyperfine coupling was not observed in  $\text{PrCu}_2\text{Si}_2$  in spite of the strong hybridization at the Si sites. This is probably due to the small CF splitting.

We have examined the effect of the temperature-dependent hyperfine coupling on the nuclear relaxation in  $\text{CeCu}_2\text{Si}_2$  and  $\text{YbCu}_2\text{Si}_2$ . The experimental findings are the followings:

- The temperature dependence of  $1/T_1$  at the Cu and Si sites significantly differs in both the compounds.
- $1/T_1T$  consists of the conduction electron contribution, which is temperature-independent and approximately equivalent to the values in  $\text{YCu}_2\text{Si}_2$  and  $\text{LaCu}_2\text{Si}_2$ , and the  $f$  electron contribution, which varies with temperature. The observed site dependence is predominantly ascribed to the conduction-electron contribution.
- In  $\text{CeCu}_2\text{Si}_2$ , the  $f$  contributions at the Cu and Si sites are proportional to each other at high temperatures, and the deviation from the linearity at low temperatures are weak. The anisotropy of  $1/T_1T$  at both the sites are almost temperature-independent.
- In  $\text{CeCu}_2\text{Si}_2$ ,  $1/T_1$  at the Cu sites is comparable to that at the Si sites, though the hyperfine coupling at the Cu sites is almost zero at high temperatures.
- On the contrary, in  $\text{YbCu}_2\text{Si}_2$ , the anisotropy at the Si sites remarkably changes in the same temperature region as the hyperfine coupling. The site dependence weakly changes in the same temperature region.

The analysis using the conventional form of  $1/T_1$  (see eq. (1.11)) has shown that it is impossible to estimate correctly the anisotropy and the site dependence of  $1/T_1$  from the hyperfine coupling even at high temperatures, where the  $f$  contributions to  $1/T_1$  at the Cu and Si sites are proportional to each other and the  $K - \chi$  plots are linear.

We have given an alternative explanation based on the hyperfine coupling due to the direct  $f$ -ligand hybridization. Considering the Curie terms in  $\chi''(q, \omega)$  have different hyperfine couplings, we qualitatively explain that the anisotropy and the site dependence of  $1/T_1$  change as the CF level occupations in  $\text{YbCu}_2\text{Si}_2$ . In  $\text{CeCu}_2\text{Si}_2$ , the anisotropy and the site dependence change weakly as temperature. In our model, this is because the excited doublets have only negligible contributions. When a Lorentzian spectrum  $\lim_{\omega \rightarrow 0} \chi''(\omega)/\omega = \chi_g/\Gamma$  is assumed, observed susceptibility or Knight shift is often used as  $\chi_g$  for the analysis of  $1/T_1$ . This is inadequate, because the susceptibility and the Knight shift consist of not only the Curie terms but also the Van Vleck terms. Alternatively, we assumed a Curie law for  $\chi_g$ , and obtained  $\Gamma$  proportional to the quasielastic line width above about 70K. We conclude that the conventional analysis of the nuclear relaxation (eq. (1.11)), using the hyperfine coupling experimentally obtained and the susceptibility

or the Knight shift, is not successful for the hyperfine coupling due to the direct  $f$ -ligand hybridization.

## References

- [1] For reviews, : *Magnetism*, ed. H. Suhl (Academic Press, New York, 1973) Vol. V, and P. Schlottmann: Phys. Rep. **18** (1989) 1.
- [2] For reviews, A. Narath: *Magnetism*, ed. H. Suhl (Academic Press, New York, 1973) Vol. V, Chap. 5, p.63, and A. Narath: CRC Crit. Rev. Solid State Sci. **3** (1972) 1.
- [3] D.V. Lang, J.B. Boyce, D.C. Lo and C.P. Slichter: Phys. Rev. Lett. **29** (1972) 776.
- [4] M.A. Ruderman and C. Kittel: Phys. Rev. **96** (1954) 99.
- [5] T. Kasuya: Prog. Theor. Phys. **16** (1956) 45.
- [6] K. Yosida: Phys. Rev. **106** (1957) 893.
- [7] G.R. Stewart: Rev. Mod. Phys. **56** (1984) 755
- [8] N. Grewe and F. Steglich: *Handbook on the Physics and Chemistry of Rare Earths*, ed. K.A. Gschneidner, Jr. and L. Eyring (North-Holland, Amsterdam, 1991) Vol. 14, p. 343.
- [9] R.E. Watson and A.J. Freeman: *Hyperfine Interactions*, ed. A.J. Freeman and R.B. Frankel (Academic, New York, 1967) p.53.
- [10] For reviews, E. Dormann: *Handbook on the Physics and Chemistry of Rare Earths*, ed. K.A. Gschneidner, Jr. and L. Eyring (North-Holland, Amsterdam, 1991) Vol. 14, Chap. 94, p.63.
- [11] S.M. Myers and A. Narath: Solid State Commun. **12** (1973) 83.
- [12] T. Shimizu, H. Yasuoka, Z. Fisk and J.L. Smith: J. Phys. Soc. Jpn. **56** (1987) 4113.
- [13] B. Coqblin and J.R. Schrieffer: Phys. Rev. **185** (1969) 847.
- [14] S. Takagi, A. Oyamada and T. Kasuya: J. Phys. Soc. Jpn. **57** (1988) 1456.
- [15] D.E. MacLaughlin: *Valence Fluctuations in Solids*, ed. L.M. Falico *et al.* (North-Holland, Amsterdam, 1981) p. 321.
- [16] V. Jaccarino, B.T. Matthias, M. Peter, H. Suhl and J.H. Wernick: Phys. Rev. Lett. **5** (1960) 251.
- [17] R. Vijayaraghavan, S.K. Malik and V.U.S. Rao: Phys. Rev. Lett. **20** (1968) 106.
- [18] T. Kasuya: *Magnetism*, ed. G.T. Rado and H. Suhl (Academic Press, New York, 1966) Vol. IIB, p. 215.
- [19] P. W. Anderson: Phys. Rev. **124** (1961) 41.
- [20] R.E. Watson, S. Koide, M. Peter and A.J. Freeman: Phys. Rev. **139** (1965) A167.
- [21] B.R. Cooper, R. Siemann, D. Yang, P. Thayamballi and A. Benerjea: *Handbook on the Physics and Chemistry of the Actinides*, ed. A.J. Freeman and G.H. Lander (North-Holland, Amsterdam, 1985) Vol. 2, p.435.
- [22] R.E. Watson and A.J. Freeman: Phys. Rev. Lett. **6** (1961) 277 [Erratum; **6**(1961)388].
- [23] H. Takahashi and T. Kasuya: J. Phys. C **18** (1985) 2697, 2709, 2721, 2731, 2745, 2755.
- [24] T. Moriya: Prog. Theor. Phys. **16** (1956) 23.
- [25] W. Rieger and E. Parthe: Monatsh. Chem. **100** (1969) 444.
- [26] A. Szytuła and J. Leciejewicz: *Handbook on the Physics and Chemistry of Rare Earths*, ed. K.A. Gschneidner, Jr. and L. Eyring (North-Holland, Amsterdam, 1989) Vol. 12, p.133.
- [27] G. Neumann, J. Langen, H. Zahel, D. Plümacher, Z. Kletowski, W. Schlabitz and D. Wohlleben: Z. Phys. B **59** (1985) 133.
- [28] K. Hiebl, P. Rogl, C. Horvath, K. Remschnig and H. Noel: J. Appl. Phys. **67** (1990) 943.
- [29] R. Feyerherm, A. Amato, C. Geibel, F.N. Gyax, P. Hellmann, R.H. Heffner, D.E. MacLaughlin, R. Müller-Reisener, G.J. Nieuwenhuys, A. Schenck and F. Steglich: Physica B **206&207** (1995) 596, and references therein.
- [30] B. Batlogg, J.P. Remeika, A.S. Cooper and Z. Fisk: J. Appl. Phys. **55** (1984) 2001.
- [31] Y. Onuki, T. Hirai, T. Komatsubara, S. Takayanagi, A. Sumiyama, A. Furukawa, Y. Oda and H. Nagano: J. Magn. Magn. Mater. **52** (1985) 338.
- [32] S. Horn, E. Holland-Moritz, M. Loewenhaupt, F. Steglich, H. Scheuer, A. Benoit and J. Flouquet: Phys. Rev. B **23** (1981) 3171.
- [33] E.A. Goremychkin and R. Osborn: Phys. Rev. B **47** (1993) 14280.
- [34] M. Ishikawa, H. Yashima, M. Takahashi, T. Satoh and M. Takigawa: J. Magn. Magn. Mater. **63&64** (1987) 351.
- [35] J. Aarts, F.R. de Boer and D.E. MacLaughlin: Physica B **121** (1983) 162.
- [36] K. Ueda, Y. Kitaoka, H. Yamada, Y. Kohori, T. Kohara and K. Asayama: J. Phys. Soc. Jpn. **56** (1987) 867.
- [37] Y. Kitaoka, H. Yamada, K. Ueda, Y. Kohori, T. Kohara, Y. Oda and K. Asayama: *Proc. 18th Int. Conf. Low Temp. Phys., Kyoto, 1987*, Jpn. J. Appl. Phys. **26** (1987) Suppl. 26-3, 1221.

- [38] T. Ohama, H. Yasuoka, D. Mandrus, Z. Fisk and J.L. Smith: *J. Phys. Soc. Jpn.* **64** (1995) 2628.
- [39] K.R. Bauchspiess, W. Boksich, E. Holland-Moritz, H. Launois, R. Pott and D. Wohlleben: *Valence Fluctuations in Solids*, ed. L. M. Falicovet *et al.* (North-Holland, Amsterdam, 1981) p. 417.
- [40] J.J. Joyce, A.J. Arko, J.M. Lawrence, J. Tang, P.C. Canfield, R.J. Bartlett, Z. Fisk, J.D. Thompson and P.S. Riseborough: *Solid State Commun.* **83** (1992) 551.
- [41] R.I.R. Blyth, J.J. Joyce, A.J. Arko, P.C. Canfield, A.B. Andrews, Z. Fisk, J.D. Thompson, R.J. Bartlett, P. Riseborough, J. Tang and J.M. Lawrence: *Phys. Rev. B* **48** (1993) 9497.
- [42] A.B. Andrews, R.I.R. Blyth, A.J. Arko, J.J. Joyce, Z. Fisk, J.D. Thompson, R.J. Bartlett, P.C. Canfield, C.G. Olson, P. Benning and P.S. Riseborough: *Physica B* **199&200** (1994) 15.
- [43] J.D. Thompson, H.A. Borges, Z. Fisk, S. Horn, R.D. Parks and G.L. Wells: *Theoretical and Experimental Aspects of Valence Fluctuations and Heavy Fermions*, ed. L.C. Gupta and S.K. Malik (Plenum Press, New York, 1987) p. 151.
- [44] E. Holland-Moritz, D. Wohlleben and M. Loewenhaupt: *Phys. Rev. B* **25** (1982) 7482.
- [45] U. Walter, E. Holland-Moritz and U. Steigenberger: *Z. Phys. B* **89** (1992) 169.
- [46] B.C. Sales and R. Viswanathan: *J. Low Temp. Phys.* **23** (1976) 449.
- [47] W. Schlabit, J. Baumann, G. Neumann, D. Plümacher and K. Reggentin: *Crystalline electric field effects in f-electron magnetism*, eds. P. Guertin, W. Suski, Z. Zolnierak (Plenum, New York, 1982) p. 289.
- [48] E.V. Sampathkumaran, I. Das, R. Vijayaraghavan, K. Hirota and M. Ishikawa: *Solid State Commun.* **78** (1991) 971.
- [49] E. A. Goremychkin, R. Osborn and A.Yu. Muzychka: *Phys. Rev. B* **50** (1994) 13863.
- [50] E.V. Sampathkumaran and I. Das: *Physica B* **186-188** (1993) 328, and references therein.
- [51] C. Routsis and J.K. Yakinthos: *Phys. Stat. Sol. A* **68** (1981) K153.
- [52] E.V. Sampathkumaran, L.C. Gupta and R. Vijayaraghavan: *J. Phys. C* **12** (1979) 4323.
- [53] T. Ohama, H. Yasuoka and E. V. Sampathkumaran: *J. Phys. Soc. Jpn.* **64** (1995) 1339.
- [54] M. Ishikawa, H.F. Braun and J.L. Jorda: *Phys. Rev. B* **27** (1983) 3092.
- [55] I.D. Weisman, L.J. Swartzendruber and L.H. Bennett: *Techniques of Metals Research*, ed. E. Passaglia (John Wiley & Sons, New York, 1973) p. 165.
- [56] E.R. Andrew and D.P. Turnstall: *Proc. Phys. Soc. London* **78** (1961) 1.
- [57] H. Yamagata: private communication.
- [58] About pulse sequences, see E.L. Hahn: *Phys. Rev.* **80** (1950) 580.
- [59] A. Abragam: *Principles of Nuclear Magnetism*, (Clarendon, Oxford, 1961).
- [60] J. Jensen, J.G. Houmann and H. Bjerrum: *Phys. Rev. B* **12** (1975) 303.
- [61] J.H. Van Vleck: *J. Chem. Phys.* **5** (1937) 320.
- [62] The ion-core diamagnetic susceptibilities are estimated from the data R.R. Gupta: *Landolt-Börnstein*, ed. K.-H. Hellwege and A.M. Hellwege (Springer-Verlag, Berlin, Heidelberg, 1986) Group II, Vol. 16.
- [63] P.S. Bagus, B. Liu and H.F. Schaefer III: *Phys. Rev. A* **2** (1970) 555.
- [64] W.B. Lewis, J.A. Jackson, J.F. Lemons and H. Taube: *J. Chem. Phys.* **36** (1962) 694.
- [65] K. Hiraoka, Y. Kasamatsu, K. Kojima and T. Hihara: *Physica B* **186-188** (1993) 535.
- [66] Y. Kohori, T. Kohara, H. Shibai, Y. Oda, T. Kaneko, Y. Kitaoka and K. Asayama: *J. Phys. Soc. Jpn.* **56** (1987) 2263.
- [67] K. Kojima, Y. Hukuda, S. Miyata, T. Takabatake, H. Fujii and T. Hihara: *J. Magn. Magn. Matter.* **104-107** (1992) 49.
- [68] S. Takagi *et al.*: unpublished.
- [69] K. Takegahara, Y. Aoki and A. Yanase: *J. Phys. C* **13** (1980) 583.
- [70] G. Zwignagl, V. Zevin and P. Flude: *Physica B* **163** (1990) 577.

